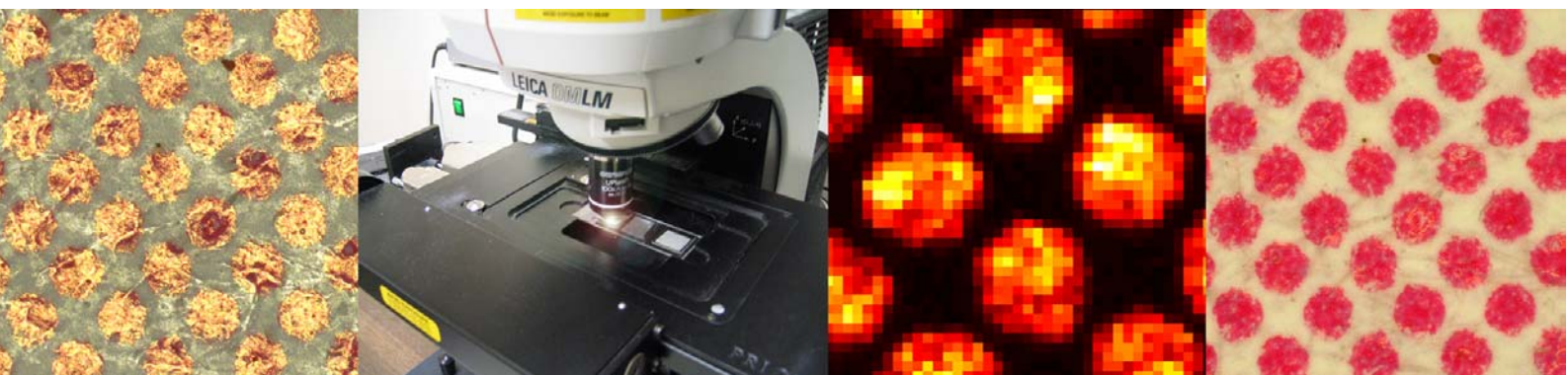


# CONFOCAL RAMAN MICROSCOPY IN CHEMICAL AND PHYSICAL CHARACTERIZATION OF COATED AND PRINTED PAPERS

Jouko Vyörykkä



TEKNILLINEN KORKEAKOULU  
TEKNISKA HÖGSKOLAN  
HELSINKI UNIVERSITY OF TECHNOLOGY  
TECHNISCHE UNIVERSITÄT HELSINKI  
UNIVERSITE DE TECHNOLOGIE D'HELSINKI

# CONFOCAL RAMAN MICROSCOPY IN CHEMICAL AND PHYSICAL CHARACTERIZATION OF COATED AND PRINTED PAPERS

Jouko Vyörykkä

Dissertation for the degree of Doctor of Science in Technology to be presented with due permission of the Department of Forest Products Technology for public examination and debate in Auditorium V1 at Helsinki University of Technology (Espoo, Finland) on the 22nd of October 2004, at 12 noon.

Helsinki University of Technology  
Department of Forest Products Technology  
Laboratory of Forest Products Chemistry

Teknillinen korkeakoulu  
Puunjalostustekniikan osasto  
Puunjalostuksen kemian laboratorio

Distribution:

Helsinki University of Technology  
Laboratory of Forest Products Chemistry  
P.O.Box 6300  
FIN-02015 HUT, Finland  
URL: <http://www.hut.fi/Units/Forestpc/>  
Tel. +358 9 4511  
Fax +358 9 451 4259

© 2004 Jouko Vyörykkä

ISBN 951-22-7230-X  
ISBN 951-22-7231-8 (PDF)  
ISSN 1457-1382  
ISSN 1795-2409 (E)  
URL: <http://lib.hut.fi/Diss/2004/isbn9512272318/>

Picaset Oy  
Helsinki 2004



HELSINKI UNIVERSITY OF TECHNOLOGY P.O. BOX 1000, FIN-02015 HUT <a href="http://www.hut.fi">http://www.hut.fi</a>		ABSTRACT OF DOCTORAL DISSERTATION	
Author Jouko Vyörykkä			
Name of the dissertation Confocal Raman Microscopy in Chemical and Physical Characterization of Coated and Printed Papers			
Date of manuscript 28.5.2004		Date of the dissertation 22.10.2004	
<input type="checkbox"/> Monograph		<input checked="" type="checkbox"/> Article dissertation (summary + original articles)	
Department	Department of Forest Products Technology		
Laboratory	Laboratory of Forest Products Chemistry		
Field of research	Forest Products Chemistry		
Opponent(s)	Dr. Umesh P. Agarwal		
Supervisor	Professor Tapani Vuorinen		
(Instructor)	Professor Tapani Vuorinen		
Abstract			
<p>In offset printing on coated papers an uneven print, mottling, is a serious problem. Uneven styrene-butadiene (SB) latex distribution may be the reason for the mottled print. In this work, confocal Raman microscopy methods were developed for chemical and physical characterization of printed and coated papers. The main emphasis was laid on analysis of the SB-latex distribution in x-y-z direction.</p> <p>A depth profiling method was developed. An immersion method was found to be essential in the depth profiling of light scattering coated papers. Model samples were employed to obtain a better understanding of the depth profiling method. The method was applied in the analysis of SB-latex migration and measurement of the thickness of paper coating layers and ink films.</p> <p>Lateral mapping of paper coatings was developed for bulk and surface analysis. In mapping of coating bulk, the whole coating layer was measured and the analysis could be done through print. Lateral mapping of the bulk layer provided information on SB-latex distribution, and variations in coat weight and ink density could be mapped simultaneously. Bulk mapping was combined with light microscopy images acquired from the same area.</p> <p>A higher magnification objective gave the means to measure the outermost 1-2 <math>\mu\text{m}</math> of the coating layer. Analysis of the coating surface is important because of the ink-coating interaction taking place on the coating surface. In the surface analysis, SB-latex content and its variation in different scales were of interest. The total areas analysed contained many areas of 1 mm x 1 mm.</p>			
Keywords Raman, depth profiling, immersion, mapping, coating, binder, migration			
UDC	672.2:676.014:676.017:543.4	Number of pages	70+28
ISBN (printed)	951-22-7230-X	ISBN (pdf)	951-22-7231-8
ISBN (others)		ISSN	1457-1382
Publisher Helsinki University of Technology, Laboratory of Forest Products Chemistry			
Print distribution Helsinki University of Technology			
<input checked="" type="checkbox"/> The dissertation can be read at <a href="http://lib.hut.fi/Diss/">http://lib.hut.fi/Diss/</a>			

## Preface

I first became acquainted with confocal Raman microscopy in late 1998 when I began work on my master's thesis at HUT. I would like to thank Professors Per Stenius and Tapani Vuorinen for giving me the opportunity to work in their research group and continue my studies on Raman spectroscopy after graduation. I would also like to thank Hanna Iitti for her skilful experimental work and the good working atmosphere she created. Mari Tenhunen, Jussi Tenhunen and Katri Vikman contributed in a major way through fruitful discussions and co-operation. Professor Douglas Bousfield kindly gave me the opportunity to participate in the Paper Surface Science Program at the University of Maine. My colleagues in the Laboratory of Forest Products Chemistry at HUT made working there a great experience. I am indebted to all of you. Finally warmest thanks to my parents and my wife Jonna for their invaluable support and patience during the years it took to complete this work.

TEKES (National Technology Agency of Finland) and other partners (Eka Polymer Latex, KCL, Metso automation, Metso paper, M-real, Myllykoski Paper, Raisio Chemicals, Specialty Minerals, Specialty Minerals Nordic, Stora Enso, UPM and VTT Electronics) are acknowledged for their contribution through TEKES projects (Profile 1998-2001, Mappi 2002 and Pinkki 2003-2004) and various contract jobs.

Jouko Vyörykkä

## List of Publications

This dissertation is a review of the author's work for the development of confocal Raman microscopy methods for chemical and physical characterization of coated and printed paper products. The work comprises this summary, with supplementary unpublished results, and the following publications, hereafter referred to by their Roman numbers I-IV:

I

Vyörykkä, J., Halttunen, M., Iitti, H., Tenhunen, J., Vuorinen, T. and Stenius, P., Characteristics of immersion sampling technique in confocal Raman depth profiling, *Applied Spectroscopy*, 56(6), 2002, p. 776

II

Vyörykkä, J., Paaso, J., Tenhunen, M., Tenhunen, J., Iitti, H., Vuorinen, T. and Stenius, P., Analysis of depth profiling data obtained by confocal Raman microspectroscopy, *Applied Spectroscopy*, 57(9), 2003, p. 1123

III

Vyörykkä, J., Bousfield, D.W. and Vuorinen, T., Confocal Raman microscopy: A non destructive method to analyze depth profiles of coated and printed papers, *Nordic Pulp and Paper Research Journal*, 19(2), 2004, p. 218

IV

Vyörykkä, J., Juvonen, K., Bousfield, D.W. and Vuorinen, T., Raman microscopy in lateral mapping of chemical and physical composition of paper coating, *Tappi Journal*, 3(9), 2004, p.

19

## Author's Contribution

The work reported in this Doctoral thesis was mainly done in the Laboratory of Forest Products Chemistry of the Helsinki University of Technology during the period 2000-2004. The author was one of the main inventors of the immersion technique and its application in confocal Raman microscopy. A patent application dealing with the immersion depth profiling method was filed by the author and co-workers in 1999 (FI 19992439, Nov. 12, 1999). The author was responsible for experimental design, programming the instrument and development of the data analysis. The manuscripts were mainly written by the author. He has also presented the results at several international conferences and in conference proceedings<sup>†</sup>.

<sup>†</sup> oral presentations at international conferences, reported in conference proceedings

1. Vyörykkä, J., Halttunen, M., Tenhunen, J., Paaso, J., Kenttä, E. and Stenius P., Confocal Raman spectroscopy in the depth profiling of paper coating colours, Paper and Coating Chemistry Symposium, Stockholm, 2000, p. 74
2. Vyörykkä, J., Halttunen, M. Iitti, H., Vuorinen, T. and Stenius, P., Confocal Raman analysis method to study binder depth profiles in coating layers, TAPPI Coating and Graphic Arts Conference and Trade Fair, San Diego, USA, 2001, p. 193
3. Vyörykkä, J., Iitti, H., Vuorinen, T. and Stenius, P., Raman microspectroscopy in the lateral mapping of paper coating composition, TAPPI Coating and Graphic Arts Conference and Trade Fair, Orlando, USA, 2002, p. 265
4. Vyörykkä, J., Alasaarela, I., Halttunen, M., Iitti, H., Tenhunen, J., Vuorinen, T. and Stenius, P., Benefits of immersion optics in confocal Raman microscopy, The XVIIth Conference on Raman Spectroscopy, Budapest, Hungary, 2002, p. 239

# Contents

<b>1</b>	<b>INTRODUCTION</b> .....	<b>7</b>
1.1	MOTTILING IN OFFSET PRINTING .....	7
1.2	RAMAN SPECTROSCOPY .....	10
1.3	OBJECTIVE OF THE STUDY .....	11
<b>2</b>	<b>MATERIALS AND METHODS</b> .....	<b>12</b>
2.1	CONFOCAL RAMAN MICROSCOPY .....	12
2.2	SAMPLES.....	14
<b>3</b>	<b>RESULTS AND DISCUSSION</b> .....	<b>18</b>
3.1	QUANTIFICATION.....	18
3.2	DEPTH RESOLUTION .....	23
3.2.1	<i>Effect of light refraction on depth resolution</i> .....	23
3.2.2	<i>Effect of light scattering on depth resolution</i> .....	24
3.2.3	<i>Determination of depth resolution</i> .....	26
3.2.4	<i>Layer thickness analysis below the nominal depth resolution</i> .....	29
3.2.5	<i>Depth resolution in binder migration studies</i> .....	31
3.3	SPATIAL RESOLUTION IN LATERAL MAPPING .....	33
3.4	DEPTH PROFILING OF COATED AND PRINTED PAPERS.....	36
3.4.1	<i>Analysis of binder migration</i> .....	37
3.4.2	<i>Coating thickness analysis</i> .....	38
3.4.3	<i>Determination of ink layer thickness</i> .....	40
3.5	LATERAL ANALYSIS OF PAPER COATINGS.....	44
3.5.1	<i>Surface mapping of paper coatings</i> .....	44
3.5.2	<i>Imaging of light scattering and reflection</i> .....	48
3.5.3	<i>Bulk mapping of paper coatings</i> .....	50
3.6	LIMITATIONS OF RAMAN MICROSCOPY IN PAPER COATING ANALYSIS .....	54
<b>4</b>	<b>CONCLUSIONS</b> .....	<b>55</b>
<b>5</b>	<b>LITERATURE</b> .....	<b>57</b>
<b>6</b>	<b>APPENDIX</b> .....	<b>66</b>

# List of Abbreviations and Mathematical Symbols

## Abbreviations

AFM	Atomic force microscopy
ATR	Attenuated total reflectance
CLC	Cylindrical laboratory coater
CMC	Carboxymethyl cellulose
CCD	Charge coupled device
ESEM	Environmental scanning electron microscopy
FWHM	Full width at half maximum
GCC	Ground calcium carbonate
HUT	Helsinki University of Technology
IR	Infrared
KCL	Oy Keskuslaboratorio – Centrallaboratorium AB
LIPS	Laser induced plasma spectroscopy
LWC	Light weight coated paper
MSP	Metered size press
NA	Numerical aperture
NIR	Near infrared
PCC	Precipitated calcium carbonate
PET	Poly(ethylene terephthalate)
PSD	Particle size distribution
PSF	Point-spread function
PPH	Parts per hundred (of dry pigment)
SEM	Scanning electron microscopy
SEM-BSE	Scanning electron microscopy with backscattered electron mode
SEM-EDS	Scanning electron microscopy with energy dispersive spectrometry
SB	Styrene-butadiene
T <sub>g</sub>	Glass transition temperature
UV	Ultraviolet
XPS	X-ray photoelectron spectroscopy

## Mathematical symbols

$D_S$	Small area variation of SB-latex content (150 $\mu\text{m}$ x 150 $\mu\text{m}$ )
$D_L$	Large area variation of SB-latex content (1 mm x 1 mm)
$\Delta x$	Lateral resolution
$\Delta z$	Depth resolution
$e$	Neper's number
$T$	Solid angle
$h$	Planck's constant
$I$	Intensity of measured light
$I_0$	Intensity of incoming light
$\zeta$	Laser wavelength
$\tau_0$	Frequency of incident light
$\tau_v$	Frequency of vibrational state
$N$	Number of scattering molecules per unit area
$n$	Refractive index
$NA$	Numerical aperture
$\omega$	Raman scattering cross-section
$s$	Focusing depth
$s'$	Depth of measurement
$Stdev$	Standard deviation
$x_n$	SB-latex:CaCO <sub>3</sub> band height ratios in an area of 1 mm x 1 mm

## **1 Introduction**

Pigmented paper coatings mainly consist of calcium carbonate or kaolin pigments and latex or starch binders. Thickeners and other additives are applied in smaller amounts (Lehtinen 2000). Air might also be considered an important component of porous paper coatings, since it makes a contribution to the optical, mechanical and fluid absorption properties (Lepoutre 1989). Coated paper grades are of particular importance for multicolour printed magazines and brochures. Offset printing is the most common printing method in the printing industry and the method used for the printing of large numbers of copies of magazines, brochures, posters, catalogues, etc. Uneven print quality, mottling, is considered as a serious problem in offset printing on coated paper grades.

### **1.1 Mottling in offset printing**

In offset printing, changes are made to the surface chemistry of lithographic printing plates; image areas are made hydrophobic and non-image areas hydrophilic (Oittinen and Saarelma 1998). Fountain water, which adheres to hydrophilic areas, is applied first (Hird 1995). Ink then covers the hydrophobic areas, which were not covered by the fountain water. The adhesion of ink in the non-image area should be lower than the ink cohesion. The presence of fountain water in the non-printing areas weakens the ink adhesion, and the force needed to remove the ink from the non-printing areas is much lower than the force needed to remove it from the printing areas (Oittinen and Saarelma 1998). Hence non-printing areas remain ink-free. From the printing plate the image is transferred to a rubber blanket and from the blanket to paper.

In multicolour offset printing, wet on wet printing, several colours are printed successively and there may not be enough time for the ink to dry completely between the printing units. A part of the ink layer is thus split and backtrapped in the blanket of the next unit (Engström 1994). If the ink sets unevenly, the backtrap will be uneven, as will the final print. The result is called backtrap mottle. Backtrap is stronger in the first down colours as these will pass through the following printing units (Engström 1994).

Another type of mottle, fountain water mottle, appears if the paper does not have enough time to absorb the fountain water applied to the non-printed area before entering the next unit

(Engström and Rigdahl 1993). The adsorption of fountain water on the paper may be uneven. The unabsorbed water prevents proper and even ink transfer in the second or later units, leading to a mottled print unit (Engström and Rigdahl 1993). Fountain water mottle is the most common type of mottle in offset printing (Engström and Rigdahl 1993).

The underlying cause of print mottle is believed to be uneven latex and pigment distribution (Lee and Whalen-Shaw 1993, Zang and Aspler 1998). These uneven distributions emerge before coating consolidation due to high absorbance of base stock or unfavourable drying conditions (Lepoutre 1989, Yamazaki et al. 1993, Engström 1994). Kim et al. (1998) studied the drying of coated paper and found, by using scanning electron microscopy (SEM), X-ray photoelectron spectroscopy (XPS) and cryo-SEM, that print mottle could be reduced by a more uniform distribution of coating chemicals and a more even microstructure on the coating surface. Coating colour dispersions having clustered latex particles have been reported to lead to a non-uniform structure of the dry coating (Van Gilder 2004). Arai et al. (1988) applied XPS in surface and depth directional investigations of pigment and binder distribution and found a correlation between fountain water mottle and non-uniform surface distribution of pigments and binders. No correlation was found with depth directional distributions. Contrary to this, computer simulations suggest that smaller latex particles enrich at the surface during coating application (Ragner 1999, Gagnon et al. 2001).

Coating thickness distribution has a major influence on the paper quality. It affects opacity, brightness, print mottle, blistering and print gloss, making coating structure analysis of great importance (Kent et al. 1986). The non-uniformity of the base paper causes variations in coat weight and creates the conditions for non-uniform binder distribution (Lee and Whalen-Shaw 1993). Using UV absorption spectroscopy for binder analysis, Engström and Lafaye (1992) concluded that uneven coat weight is associated with uneven binder distribution at the coating surface. Allem (1998) found by SEM method a direct correlation between print quality and coating thickness uniformity of light weight coated papers. Gane (1989) reported that only gross variations in base sheet absorbency cause binder migration that independently leads to print mottle, while heterogeneity in the coating structure and drying are the more likely causes of macroscopic print mottle.

Recent publications suggest that print mottle may be related more to the structural properties of the paper coating than to latex migration. Xiang and Bousfield (2001) found ink setting rates to decrease with increasing coat weight. Groves et al. (2001) found water soluble components of coating colours to enrich in the top layer of the paper coating and suggested that several earlier studies may have mistakenly measured water soluble surfactants rather than latex content. Xiang et al. (2000) showed that mottle appeared in papers with “closed” regions on the surface while the latex distribution was uniform.

Several methods have been applied in styrene-butadiene (SB) latex analysis. UV absorption spectroscopy has been applied in the determination of content, but the depth sampled and the structural properties of the sample have an effect on the results (Fujiwara and Kline 1987). Many of the experimental methods applied to determine SB-latex content in depth direction require grinding or physical sectioning of the sample, and in several cases binder labelling is needed (Zimmermann et al 1995, Guyot et al 1995, Häkkänen 1998, Kenttä et al. 2000, He et al. 2002). Surface analysis of coated papers by XPS gives a sampling depth (5-10 nm) that in SB-latex measurement could be sensitive to the migration of water-soluble surfactants and dispersants (Groves et al. 2001). Kugge (2003) employed a combination of atomic force microscopy (AFM) and environmental secondary electron microscopy (ESEM) to measure SB-latex film formation and migration. The analysis area of AFM is limited, however, and there are limitations in quantification. Attenuated total reflectance infrared spectroscopy (IR/ATR) has a sampling depth of approximately 2  $\mu\text{m}$  and it has been applied in SB-latex analysis (Halttunen et al. 2001). The method requires a multivariate calibration, however, and the SB-latex signal is relatively weak. In sum, all of the earlier methods employed in SB-latex analysis have limitations in giving quantitative information from heterogeneous paper coatings. Although many studies have been done on print mottle, a lot of questions are unanswered and the need for better method remains.

The burnout method is frequently applied in the analysis of coat weight distribution. In a recent investigation SEM employed in backscattered electron mode (SEM-BSE) was preferred to burnout because the base paper contributes to the burnout results (Forsström 2003). Laser induced plasma spectroscopy (LIPS) reveals coat weight distribution without the need for physically sectioning of the sample before the measurement (Häkkänen 1999).

## 1.2 Raman spectroscopy

The Raman effect was discovered in 1928 and the first Raman microscopes were described in 1974 (Turrell and Dhamelincourt 1996). Raman spectroscopy measures scattered light. Figure 1 compares the different scattering events observed in Raman spectroscopy with the light absorption in IR spectroscopy. In Raman spectroscopy an intense monochromatic laser radiation excites a molecule to a virtual state. In an inelastic Stokes Raman scattering event the excited molecule relaxes to a higher vibrational level and the emitted photon has lower energy than the exciting laser light. Usually the Stokes region of the Raman spectrum is more intense than the anti-Stokes region since most of the molecules are on the ground vibrational level at room temperature (Lin-Vien et al. 1991).

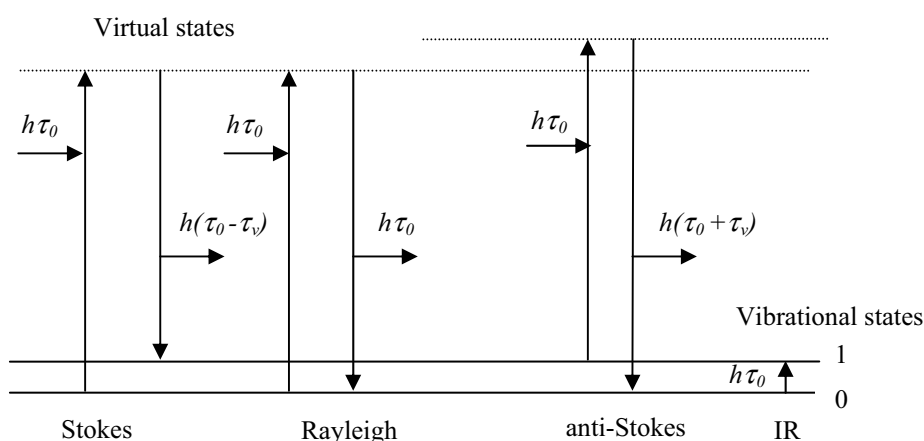


Figure 1. Schematic drawing of vibrational energy states and light energies involved in Raman and IR spectroscopies. ( $\tau_0$  = frequency of incident light,  $\tau_v$  = vibrational frequency,  $h$  = Planck's constant)

In confocal Raman microscopes, the Raman spectrometer is usually attached to a light microscope. The depth resolution and optical slicing of a sample are provided by a pinhole that restricts the signals emerging from out-of-focus zones (Turrell and Dhamelincourt 1996). The Raman scattered light is collected with the same objective through which the excitation is carried out. Typically, backscattering geometry is employed in Raman microscopy, making it possible to measure the Raman spectrum from the sample surface without sample preparation. Raman scattering is a very weak phenomenon and the recent improvements in instrumentation have been essential to make confocal Raman microscopy a well-established method of chemical analysis in the field of molecular spectroscopy. Confocal Raman microscopy has been extensively applied in the depth profiling of polymer films (Tabaksblat et al. 1992,

Hajadoost and Yarwood 1996, Hajadoost et al. 1997, Schrof and Häußling 1997, Sacristán et al. 2000, Belaroui et al. 2000).

The number of investigations where Raman spectroscopy is applied to the analysis of paper products is increasing. Older Raman studies focused on the identification of constituents of old paintings, manuscripts and artwork (Turrell and Dhamelincourt 1996). More recently Raman spectroscopy has been used to identify pigments such as calcium carbonate, talc, gypsum, titanium dioxide and kaolin in recycled paper pulp (Niemelä et al. 1999). It has also been extensively applied in pulp and bleaching investigations (Agarwal and Atalla 1995, Halttunen et al. 2001). A Raman microscope was employed in the analysis of the spatial distribution of SB-latex at the surface of a paper coating layer (Guyot et al. 1995), and confocal Raman microscopy has several times been utilized in SB-latex distribution analysis in x-y-z direction (Vyörykkä 1999, He et al. 2002, Sundqvist 2003, Bitla et al. 2003, Paper III, Paper IV). Very recent confocal Raman microscopic depth profiling work has focused on ink jet and electrophotographic printed paper products (Vikman and Sipi 2003).

### **1.3 Objective of the study**

The objective of the present work was to develop Raman microscopy for chemical and structural analysis of paper coatings in x-y-z direction. The main focus was quantitative analysis of the distribution of SB-latex. The work falls roughly into two parts: development of depth profiling and development of lateral mapping methods. The lateral mapping can further be divided into surface mapping and bulk mapping of paper coatings.

## 2 Materials and Methods

### 2.1 Confocal Raman microscopy

The majority of the Raman spectra were collected with a dispersive Kaiser Optical Systems HoloLab Raman microscope (Figure 2). The exciting light from a 785 nm GaAlAs diode laser was coupled to an Olympus BX 60 microscope with an optical fibre. This set-up gave a random laser light polarization at the sample. The laser power at the sample stage was 35 mW. The pinhole size was determined by the core diameter of the collection fibre (15  $\mu\text{m}$ ). In the HoloLab Raman microscope, the combination of a multiplexed transmission grating and a multichannel CCD array detector allows simultaneous collection of the spectral range 100-3500  $\text{cm}^{-1}$  at 4  $\text{cm}^{-1}$  spectral resolution. A typical collection time for a Raman spectrum of a paper coating with cosmic ray removal was 20 seconds.



Figure 2. HoloLab Raman microscope.

Another confocal Raman microscope employed in this work was a Renishaw RM 1000. The excitation source was a diode laser operating at wavelength of 785 nm. The measured laser power at the sample stage was 16 mW. The confocal pinhole was replaced by a combination of a slit and CCD area (Williams et al. 1994). In the RM 1000 instrument the spectral range of a static scan measurement is limited to approximately 560 wavenumbers. Extended scan mode would have given the whole wavenumber range, but the measurement would have been relatively time consuming. A typical collection time for a static scan Raman spectrum of a paper coating was 60-90 seconds.

Depth profiling measurements were carried out by stepwise (1  $\mu\text{m}$ ) focusing of the exciting laser inside the sample and the collection of a separate Raman spectra at each z-slice. The depth axis zero point was the starting point of the depth profiling and the distance between the starting point and the actual surface varied in the measurements.

Immersion depth profiling measurements were carried out with a 100X (NA 1.30) oil-immersion objective (Olympus, universal plan fluorite) having 100  $\mu\text{m}$  working distance. In the HoloLab Raman instrument the movement of the focal point in the z-direction was accomplished with a Physik Instrumente PIFOC piezo objective scanner (P-721.10) having 100  $\mu\text{m}$  scanning range and a full range repeatability of  $\pm 20$  nm. The RM 1000 Raman instrument was supplied with an encoded motorized x-y-z stage with 0.1  $\mu\text{m}$  repeatability.

In studies in the lateral direction, the sample stage of the HoloLab Raman instrument was controlled with a Coherent EncoderDriver actuator system (37-0486). The unidirectional repeatability of this system was 0.1  $\mu\text{m}$  and the stroke length of the x-y stage was 9 mm. In lateral mapping of the paper coating surface with the HoloLab instrument, a second motorized x-y stage (Physik Instrumente, M.410GC & M.415GC) having 100 mm x 150 mm stroke length was used. In surface mapping, automatic focusing was accomplished with the piezo objective scanner that was also used in the depth profiling.

Light scattering and reflection images were acquired with the light microscope attached to the HoloLab Raman instrument. A standard polarizer and an analyser were obtained from Olympus. The polarization plane of the analyser could be rotated. A digital camera (Olympus, DP12) was installed to the microscope for imaging. A low magnification objective (Olympus, 5X) was applied to cover larger areas in a single measurement.

## 2.2 Samples

Below is the list of samples that were used for calibration purposes and spatial resolution measurements and the samples that were obtained from industry to demonstrate the new Raman depth profiling and mapping methods.

*Sample set 1.* Coatings containing SB-latex, needed to calibrate the HoloLab instrument, were prepared from two pigment mixtures. The applied SB-latex (Dow, DLL 966) contents were 3, 6, 9, 12, 15 and 18 parts per hundred (pph) of dry pigment. In one series, the pigment was 100 pph of CaCO<sub>3</sub> (Omya, Hydrocarb 90) and in the other the pigment mixture was 50 pph of CaCO<sub>3</sub> and 50 pph of kaolin (Huber, Hydragloss 92). All the coatings contained 1 pph of carboxymethyl cellulose (CMC) (Noviant, Finnfix 10). The coating colours were applied on a glossy PET (polyethylene terephthalate) film with a laboratory coater using a 60 µm slit rod. The samples were dried at room temperature.

*Sample set 2.* Coatings containing CaCO<sub>3</sub> pigments (Omya: Hydrocarb 60, Hydrocarb 90 and Setacarb 97% < 2 µm) and 12 pph of SB-latex (Dow, DLL 966) were prepared for Raman intensity study on different pigment sizes. These samples were spread on a glossy PET with a laboratory slit rod coater using a 60 µm rod. The samples were dried at room temperature.

*Sample set 3.* SB-latex (Dow) samples with different T<sub>g</sub> values and gel contents were dried and measured with the HoloLab Raman microscope to determine the effect of type of SB-latex. The T<sub>g</sub> values were 4 °C, 20 °C and 24 °C. The gel content was high for the samples having T<sub>g</sub> 5 °C and 24 °C and medium for the sample with T<sub>g</sub> 20 °C.

*Sample 4.* A model coating contained 100 pph of CaCO<sub>3</sub> (Omya, Hydrocarb 90), 12 pph of SB-latex (Dow, DLL 966) and 1 pph of CMC (Noviant, Finnfix 10) was used to demonstrate the difference between traditional and immersion depth profiling of a paper coating. The coating was spread on a 10 µm PET film with a laboratory slit rod coater. The coating thickness was approximately 5 µm.

*Sample 5.* A 12 µm PET film (Wihuri Wipak) was used for determination of the point-spread function (PSF).

*Sample 6.* A double coated paper with the target coat weight of  $2 \times 9 \text{ g/m}^2$  per side was prepared for cross-section analysis. The coating contained 100 pph of  $\text{CaCO}_3$  (Omya, Hydrocarb 90), 12 pph of SB-latex (Dow, DLL 966) and 1 pph of CMC (Noviant, Finnfix 10). Coatings were produced with a cylindrical laboratory coater (CLC) at a rate of 600 m/min using constant IR drying conditions.

*Sample set 7.* Two double coated samples A and B obtained from Specialty Minerals Nordic Oy AB were used for depth profiling through print. The coating formulation and base papers were the same, but different drying conditions were applied. The precoating contained ground calcium carbonate (GCC) with a steep particle size distribution as a pigment and SB-latex as a binder. In the top coating the pigment was precipitated calcium carbonate (PCC) and the binder was SB-latex. These samples were printed in a five-colour sheet-fed offset press and depth profiled through the magenta ink test area (100% coverage). Twenty depth profiles were measured from each sample.

*Sample set 8.* Two double coated samples provided by Specialty Minerals Inc were used for measurement of thickness profiles. One sample was precoated with a metered size press (MSP, 900 m/min) and the other with a jet applicator followed by metering with a blade (1000 m/min). The precoating applied with MSP consisted of 100 pph of calcite PCC, 8 pph of SB-latex (Dow, CP 620NA) and 8 pph of starch (Penford, 280). The particle size distribution (PSD) of the calcite PCC was such that 90% of the particles by weight were smaller than  $1.10 \text{ }\mu\text{m}$  (i.e.  $\text{PSD}_{90} = 1.10 \text{ }\mu\text{m}$ ) and  $\text{PSD}_{20}$  was  $0.35 \text{ }\mu\text{m}$ . The precoating applied with blade coater was similar. The coat weights of both precoatings were  $6.5 \text{ g/m}^2$ . The top coating of both samples was applied with a blade coater (1000 m/min) and the coat weight was again  $6.5 \text{ g/m}^2$ . The top coating recipes were the same, 100 pph of aragonite PCC ( $\text{PSD}_{90} = 0.86 \text{ }\mu\text{m}$ ,  $\text{PSD}_{20} = 0.18 \text{ }\mu\text{m}$ ), 9 pph of SB-latex (Dow, CP 620NA) and 7 pph of starch (Penford, 280). The top coat calendering (1000 m/min) was performed by a gentle on-line soft nip calender at  $250 \text{ }^\circ\text{C}$  (Nip 1:  $110 \text{ kN/m}$ , Nip 2:  $40 \text{ kN/m}$ ). According to the manufacturer, typical mean pore size for the calcite PCC is  $0.110 \text{ }\mu\text{m}$  and for the aragonite PCC  $0.095 \text{ }\mu\text{m}$ . In another set of similar samples, also provided by Specialty Minerals Inc, 10 pph of rutile  $\text{TiO}_2$  was present in the precoating, which was an additional marker to differentiate between the top coating and precoating.

*Sample set 9.* The relationship between coating thickness and Raman intensity was explored with coatings spread with a laboratory slit rod coater on a glossy PET substrate. Average thicknesses were 1.5  $\mu\text{m}$ , 2.5  $\mu\text{m}$ , 7.5  $\mu\text{m}$ , 11.5  $\mu\text{m}$  and 19  $\mu\text{m}$ . These coatings contained 100 pph of  $\text{CaCO}_3$  (Omya, Hydrocarb 90) and 12 pph of SB-latex (Dow, DLL 966).

*Sample 10.* A lateral map was measured from a printed paper sample. A fine paper containing calcium carbonate was coated on a pilot coater at 800 m/min at KCL, Espoo, Finland. The coating colour contained 50 parts pph of calcium carbonate (Omya, Hydrocarb 90), 50 pph of kaolin (Huber, Hydragloss 90), 15 pph of SB-latex (Dow, DLL 966), and 0.7 pph of CMC (Noviant, Finnfix 10). The solids content of the coating colour was 65% and the target coat weight was 12  $\text{g}/\text{m}^2$ . The coated paper was calendered and printed in a four-colour sheet-fed offset press at KCL. Lateral mapping was performed from an area having 40% coverage of magenta ink.

*Sample 11.* A coated paper sample obtained from industry was used for measurement of a map from an area of coating bulk 1.75 mm x 2.25 mm. The coating contained  $\text{CaCO}_3$  and SB-latex. Raman mapping was done from a printed area having 100% coverage of magenta.

*Sample 12.* An unprinted sample obtained from Specialty Minerals Nordic Oy AB was used for large area mapping of coating bulk and light scattering measurements. The sample composition was otherwise the same as given in the description of sample set 7.

*Sample 13.* A pilot coated paper sample with strong mottle (expert ranking: 5, scale 1-5) was measured in high and low print density areas. The paper was coated at 22  $\text{g}/\text{m}^2$  per side with 50 pph of high brightness clay, 10 pph of calcined clay, 40 pph of GCC, 14 pph of SB-latex, 2 pph of starch and smaller amounts of other typical additives. The drying consisted of gentle IR drying immediately after the coating and subsequent hard air drying. The sample was the same as employed in earlier studies by Xiang et al. (1999) and Xiang et al. (2000) (their sample G).

*Sample 14.* A sample coated with a pilot coater equipped with a jet applicator at KCL, at a coater speed of 1500 m/min, was used to demonstrate the surface analysis. Pilot coated paper was supercalendered using constant speed (850 m/min) and nip load (200 kN/m). The base

paper was 41 g/m<sup>2</sup> mechanical LWC-base paper from a Finnish paper mill. The coating consisted of 100 pph of CaCO<sub>3</sub> (Omya, Hydrocarb 60), 11 pph of SB-latex (Dow, DL 940) and 1.5 pph of starch (Raisio Chemicals, Raisamyl 150 E), 0.4 pph of CMC (Noviant, Finnfix 10) and 0.3 pph of optical brightener (Bayer, Blankophor P). The target solids content of coating colour was 64% and the target pH was 8. The analysed coat weight was 12.9 g/m<sup>2</sup> and the mean pore diameter of the coating layer was 0.149 µm.

*Sample 15.* This sample was produced in similar conditions to sample 14, but it had finer CaCO<sub>3</sub> pigment (Omya, Setacarb). The sample was employed in surface analysis. The analysed coat weight was 12.7 g/m<sup>2</sup> and the mean pore diameter of the coating layer was 0.070 µm.

### 3 Results and Discussion

#### 3.1 Quantification

The intensity of Raman scattering is described by the equation

$$I = N I_0 \left( \frac{d\sigma}{d\Omega} \right) \quad (1)$$

where  $N$  is the number of scattering molecules per unit volume,  $I_0$  is the intensity of the incident laser beam and  $\frac{d\sigma}{d\Omega}$  is the differential scattering cross-section (Spiekermann 1995).

If the intensity of the laser beam is constant the intensity of the scattering is directly proportional to the number of scattering molecules. Quantitative work with Raman spectroscopy relies on linear superposition where single component Raman spectra make up the Raman spectrum of the mixture. Chemical interactions may change the molecular specimen, and in such cases linear superposition will not work (Pelletier 2003). Usually the intensities of the bands are proportional to molecular concentrations (Schrader 1995).

Raman intensities are affected by many experimental factors and thus internal standards are usually required in quantitative work (Hendra 1996). Often a compound already present in the sample can be employed as the internal standard. Sometimes an internal standard can be added. Quantification based on the use of an external standard employs unnormalised Raman spectra and controlled measurement conditions are required. While controlled conditions can be achieved in a single measurement, they are more difficult to achieve in automatic mapping. In principle, the use of external standards easily becomes impossible if the external standard and the sample do not fill the measurement volume. The measurement volume is readily changed by light scattering, and this is the case in SB-latex analysis. In the present work analysis was made of the SB-latex band at  $998 \text{ cm}^{-1}$  originating from the ring breathing of the styrene unit (Lin-Vien et al. 1991) and the  $\text{CaCO}_3$  band at  $1084 \text{ cm}^{-1}$  originating from C=O in phase stretching (Bougeard 1995). The latter can be used as an internal standard in the quantitative analysis as, generally, the coating recipe is given as the dry amount of various components relative to the dry amount of pigment (Lehtinen 2000).

Usually band areas are preferred over band heights in quantitative analysis (Spiekermann 1995). However, the signal to noise ratio may be lower for band areas than band heights if the dominating noise is random variation in the baseline (Pelletier 2003). Band height analysis gives more reliable results when partial overlapping of two Raman bands occurs (Pelletier 2003). Partial overlapping of bands of cellulose ( $1094\text{ cm}^{-1}$ ) and  $\text{CaCO}_3$  ( $1084\text{ cm}^{-1}$ ) occurs frequently due to the vicinity of the fibres in the base paper and the coating. In our case, better repeatability was obtained for coated paper samples by using band heights. Moreover, heterogeneous paper coating samples tend to have variable baselines from point to point, which means that finding general fitting parameters for band area calculations would be complicated. For small numbers of Raman spectra, individual fitting would overcome these problems, but for Raman maps containing hundreds or even thousands of Raman spectra the work would be time consuming. Moreover, slightly different parameters for curve fitting would lead to different results each time.

Raman bands are usually narrow. Figure 3 displays a typical Raman spectrum of a paper coating containing 100 pph of  $\text{CaCO}_3$  and 15 pph of SB-latex. Starch, CMC and other additives applied in smaller quantities are not usually detected owing to the insensitivity of the Raman method for weakly polarizable molecules. The partial insensitivity and linear superposition mean that the Raman bands of coated papers can be assigned relatively easily by using model compounds or literature data. Raman bands at  $279\text{ cm}^{-1}$ ,  $709\text{ cm}^{-1}$  and  $1084\text{ cm}^{-1}$  were assigned to  $\text{CaCO}_3$  (calcite), whereas the Raman bands at  $619\text{ cm}^{-1}$ ,  $998\text{ cm}^{-1}$  and  $1028\text{ cm}^{-1}$  are for SB-latex.

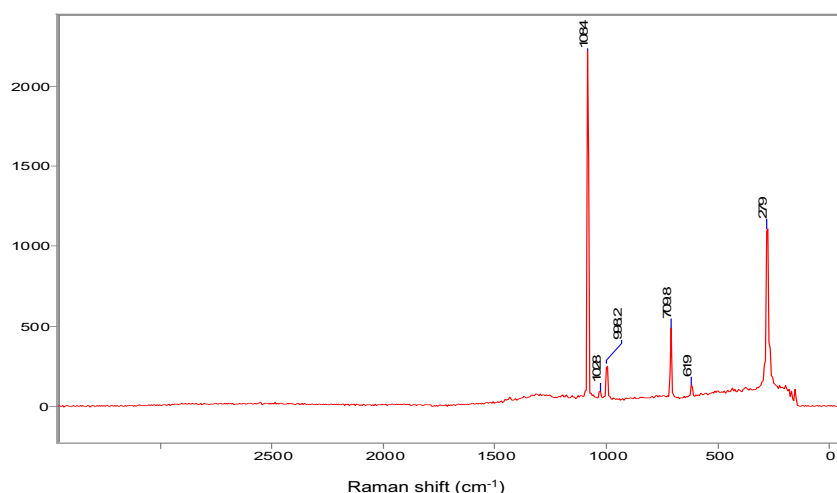


Figure 3. Raman spectrum of a coating containing  $\text{CaCO}_3$  (100 pph) and SB-latex (15 pph) measured with a dry 100X (NA 0.95) objective. Acquisition time was 20 s.

Figure 4 presents SB-latex:CaCO<sub>3</sub> band height ratios obtained for the two series of sample set 1. The difference in the slopes of the two lines is a natural consequence of the different amounts of CaCO<sub>3</sub> in the coatings. The linearity of the calibration means that it is possible to perform a semi-quantitative analysis of differences in SB-latex concentration without calibrating the instrument.

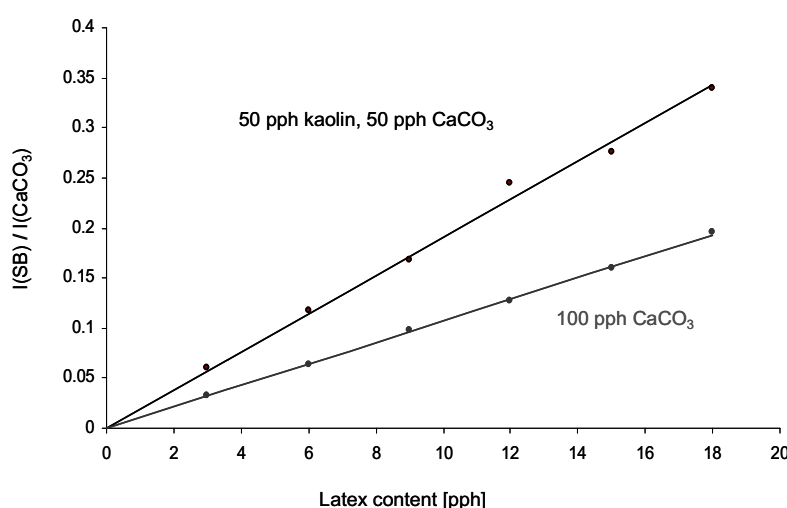


Figure 4. Calibration lines measured with the HoloLab Raman instrument. SB-latex content of the model coatings was varied, while the pigment composition (100 pph CaCO<sub>3</sub> or 50 pph kaolin – 50 pph CaCO<sub>3</sub>) was kept constant.

Repeating the measurement at the same point and analysing the intensity variance gives the repeatability of the measurement (Pelletier 2003). Ten measurements were repeated at the same position (sample 14) with a typical acquisition time (20 s). The standard error for the latex:pigment band height ratio was 2.8%. This error describes the random noise in a single measurement (Pelletier 2003).

The error for the quantification was determined from the calibration curve (Figure 4) by using linear regression analysis. For 10 pph SB-latex level the error was 0.16 pph for the coating with 100 pph CaCO<sub>3</sub>, and 0.50 pph for the coating containing 50 pph of CaCO<sub>3</sub>. The magnitude of the error depends on the experimental set-up and acquisition parameters.

Table 1 lists the SB-latex:CaCO<sub>3</sub> band height ratios for sample set 2 representing different types of CaCO<sub>3</sub>. The SB-latex content (12 pph) was the same in all samples. The coating layer could be removed from the glossy PET substrate and the latex level could be measured directly from both surfaces. Similar SB-latex levels were observed on the two surfaces. Light

scattering was not expected to have an effect on the intensity ratios because the probability of scattered light producing Raman scattered photons depends on the mass ratios of the substances as in non-scattering case. This was observed experimentally in a comparison of ratio values measured by immersion and traditional techniques. Any difference in the calculated band height ratio should be then due to the CaCO<sub>3</sub>. A change in the crystalline environment may give rise to a different response in Raman technique.

Table 1. SB-latex:CaCO<sub>3</sub> band height ratios for coatings containing different types of CaCO<sub>3</sub> and constant SB-latex level (12 pph).

	I(SB)/ I(CaCO <sub>3</sub> ) x 100 (95% confidence interval)
Hydrocarb 60	11.2 (± 1.8)
Hydrocarb 90	11.9 (± 1.2)
Setacarb	13.6 (± 0.8)

The Raman band of SB-latex at 998 cm<sup>-1</sup> is due to its styrene units. Thus a change in the styrene content of the SB-latex should affect the band height ratio. For pure SB-latex, both styrene and butadiene Raman bands were observed (Figure 31 / Appendix). Samples of sample set 3 containing pure latex were obtained from an SB-latex manufacturer to assess the effect of type of SB-latex. For pure SB-latex the peaks detected at 1664 cm<sup>-1</sup> and 1650 cm<sup>-1</sup> could be assigned to butadiene and the peak at 1601 cm<sup>-1</sup> to styrene (Bauer et al. 2000). In this case, peak areas were analysed in terms of the possible differences in the butadiene peak widths due to different degree of cross-linking in the SB-latex. The styrene to butadiene band area ratio correlated with T<sub>g</sub> of the latex (Figure 5), as expected (Lee 2000).

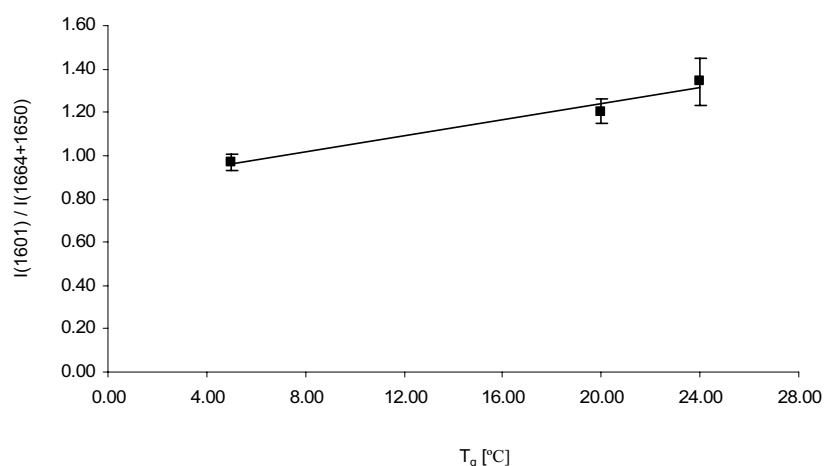


Figure 5. Styrene to butadiene peak area ratios of pure SB-latex samples measured with the HoloLab Raman instrument. The area of the 1601  $\text{cm}^{-1}$  band for styrene and the sum of the areas of two bands (1664  $\text{cm}^{-1}$ , 1650  $\text{cm}^{-1}$ ) for butadiene were employed. The gel content was high for  $T_g$  5 °C and 24 °C, but for  $T_g$  20 °C it was medium.

In conclusion, differences in the type and composition of the pigment and  $T_g$  of the latex cause differences in the SB-latex:CaCO<sub>3</sub> band intensity ratio and have an effect on the calibration. If the coating recipes are similar, however, semi-quantitative comparison of the SB-latex content is possible because the calibration line is linear. If the recipes are different, a set of calibration samples needs to be prepared and measured to obtain valid calibration coefficients.

### 3.2 Depth resolution

In confocal Raman microscopy the depth resolution is, in principle, determined mainly by the laser wavelength, the objective and the pinhole size that restricts the Raman scattering from out-of-focus zones (Tabaksblat et al. 1992). The theory of depth resolution in confocal Raman microscopy is essentially similar to the theory of confocal microscopy described by Wilson (1990). For the depth resolution the physical limit can be estimated by

$$\Delta z \approx \frac{4.4n\zeta}{2\phi(\text{NA})^2}, \quad (2)$$

where  $n$  is the refractive index of the sample,  $\zeta$  is the laser wavelength and NA is the numerical aperture of the objective (Turrell and Dhamelincourt 1996). A dry 100X objective with NA = 0.95 and laser wavelength 785 nm gives a theoretical depth resolution of 0.9  $\mu\text{m}$  when the refractive index of the sample is 1.5.

#### 3.2.1 Effect of light refraction on depth resolution

Light refraction at the air-sample interface affects the depth sampled and the nominal depth resolution (Figure 6). Recently, several publications have suggested ways to calculate and model the effects burdening confocal Raman depth profiling (Everall 2000, Baldwin and Batchelder 2001, Reinecke et al. 2001, Baia et al. 2002). However, after a drastic decrease in depth resolution due to refraction it is difficult to gain back the lost resolution mathematically.

The air-sample interface can be removed by using an oil immersion objective. An oil immersion objective for confocal Raman depth profiling has been introduced only very recently (Vyörykkä et al. 1999, Vyörykkä 1999, Everall 2000, Paper I). These publications report clear advantages of the immersion method over the traditional dry method. Recently, depth profiling with the immersion method was successfully applied in investigations of light and water fastness of ink jet prints and the adhesion of electrophotographic prints (Vikman and Sipi 2003).

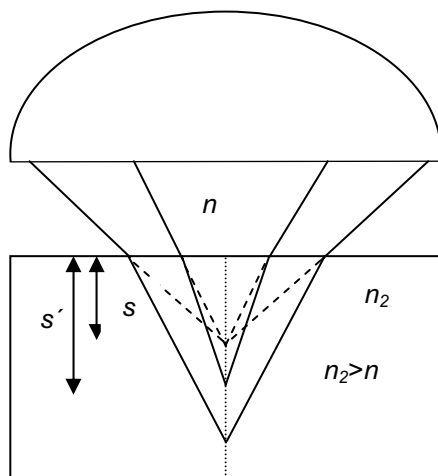


Figure 6. Refraction of focused light at air–sample interface. The difference in refractive indices causes aberration and decreases the depth resolution. The depth of measurement ( $s'$ ) in the sample is deeper than the focus point in the ideal case ( $s$ ) and the focus is blurred (Paper I).

### 3.2.2 Effect of light scattering on depth resolution

Figure 7 demonstrates the depth profiling of a paper coating (sample 4) by traditional dry Raman microscopy. The signal from the PET substrate is very weak, indicating major difficulties in the depth profiling of the pigmented coating due to its strong light scattering ability. Pigmented paper coatings are indeed designed to scatter light strongly and restrict light penetration. The traditional dry method is surface sensitive therefore. In the immersion method the sample is wetted and light scattering is greatly decreased (Paper I). Figure 8 presents a depth profile measured with the immersion technique showing that it is possible to obtain a depth profile of the PET substrate even through the coating layer. The difference between traditional and immersion depth profiling is dramatic. The traditional dry depth profiling of a paper coating is surface sensitive and depth profiling is impossible; the immersion method provides a depth profile of the coating layer as well as a depth profile of the PET substrate.

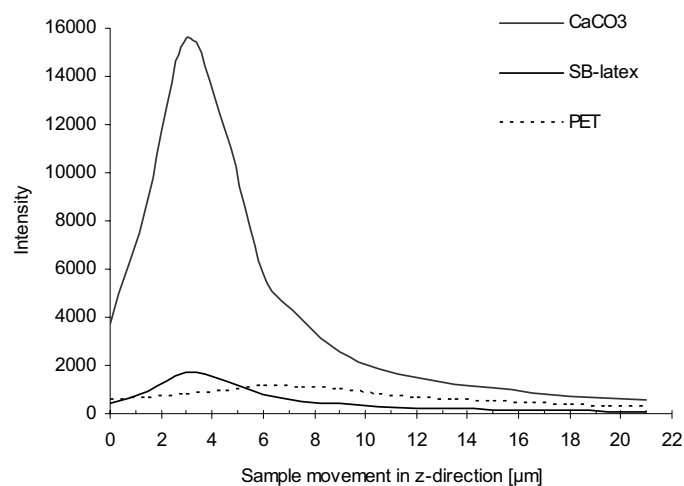


Figure 7. Depth profile of a paper coating applied on a PET film measured by the traditional dry method. The signal from the PET substrate is very weak. (Paper I)

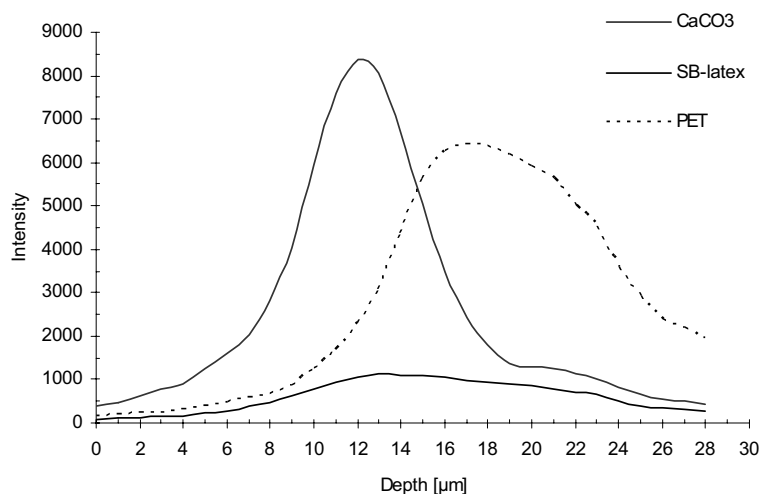


Figure 8. Depth profile of a coating applied on a PET film measured by the immersion method. The depth profile of the PET substrate can be obtained even through the coating layer. The shoulders in the  $\text{CaCO}_3$  and SB-latex profiles are due to the overlapping of Raman bands from PET. (Paper I)

The immersion method provides several advantages over the traditional dry method: depth resolution is enhanced, data analysis is easier (depth of analysis is the same as focusing depth) and fluorescence is effectively quenched (Paper I). Moreover, in the case of coated paper products, depth profiling is not possible without the reduction in light scattering provided by the immersion technique (Paper I).

### 3.2.3 Determination of depth resolution

The most popular definition of spatial resolution for a confocal system is the full width at half-maximum (FWHM) intensity of the measured instrument point-spread function (PSF) (Wilson 1990, Tabaksblat et al. 1993). The PSF describes the measurement volume. The FWHM criterion states that two triangular-shaped lines are resolved if the distance between the lines is equal to or greater than FWHM (Griffiths and de Haseth 1986). Two layers with different Raman spectra can nevertheless be detected and resolved below the depth resolution limit because the Raman signals are detected at different wavenumbers. The depth resolution does not indicate the thinnest layer that can be identified, which depends on the sensitivity of the instrument for the specimen in question. In confocal Raman spectroscopy, the final shape of the depth profile is affected by the sample thickness and concentration profiles. These variables thus have an effect on the spatial resolution obtained. Shorter excitation wavelength would improve the depth resolution (see eq. 2), but the probability of light induced fluorescence increases with the energy of the light and may ensue severe problems. It has also been suggested (Paper II) that deconvolution enhances the depth resolution of confocal Raman and that might allow a direct analysis of the concentration profiles.

A convolution integral was applied to model the depth profile formation in confocal Raman microscopy (Paper II). Figure 9 depicts a PSF (FWHM 4  $\mu\text{m}$ ), a theoretical sample function (boxcar of 20  $\mu\text{m}$  thickness) and the resulting depth profile. When the sample is considerably thicker than the width of the PSF, the sample surface is located at the half height of the maximum intensity. This corresponds to a situation where the laser is focused on the surface and half of the PSF is inside the sample (Figure 9).

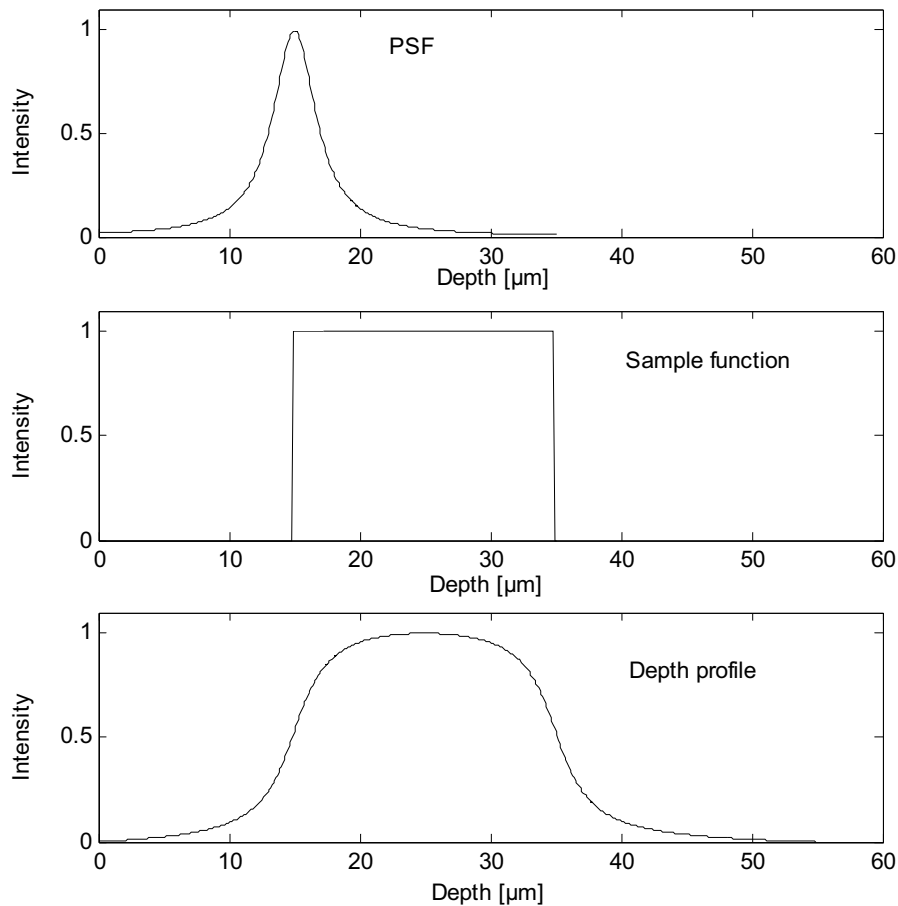


Figure 9. Signal formation in confocal Raman microscopy. The PSF is convolved over the sample function producing the depth profile of the sample. When the laser is focused on the surface, half of the PSF is inside the sample (thick sample) and the signal is half of the maximum. Hence, the sample surface is located approximately at the half height position of the depth profile.

Usually the PSF has been measured by depth profiling a thin sample to see the effect of broadening directly. Silicon wafers have been employed in Raman spectroscopy (Hajadoost and Yarwood 1996). When a silicon wafer was used, broadening of the PSF was observed and mirroring of the PSF was necessary (Paper I). The determined depth resolution was 5  $\mu\text{m}$ . Later, in Paper II, it was found that for excitation wavelength 785 nm, as employed in this work, silicon has a penetration depth ( $I = I_0/e$ ) of approximately 8  $\mu\text{m}$  and silicon wafer does not, therefore, act as a thin sample (Aspnes and Studna 1983). Knowledge of the PSF is needed to determine the depth resolution and to model the depth profiling. The PSF is also necessary if the depth resolution is to be improved by deconvolution (Govil et al. 1993, Paper II).

In Paper II it was shown that the PSF calculated from the convolution integral is the first derivative of the depth profiling curve. The film needs to be considerably thicker than the depth resolution. When the PSF passes through the front surface of a sample, a positive peak is observed in the first derivative (Figure 10). Analogously a negative peak is observed in the back surface. The distance between the maximum and the minimum of the first derivative, or between zero crossings of the second derivative, determines the sample thickness. Derivation results in image sharpening and better edge detection. In image processing, derivatives are commonly applied in edge detection (Gonzalez and Wintz 1987).

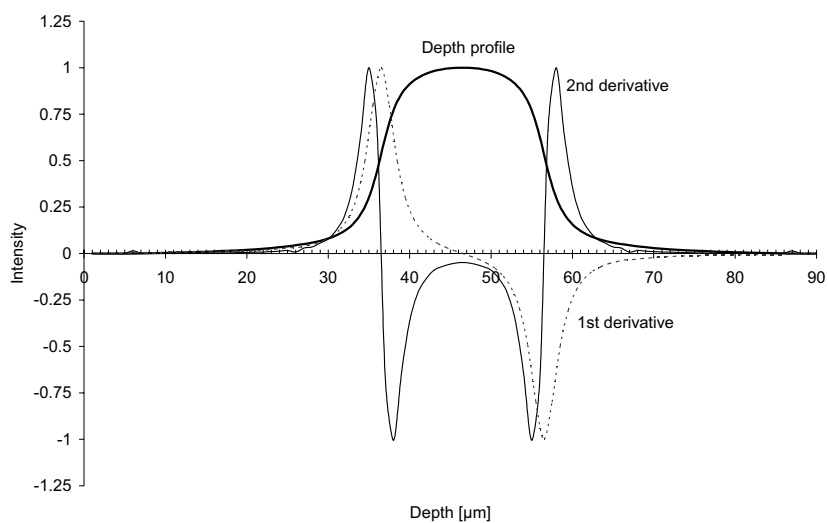


Figure 10. A theoretical Raman depth profile of a 20  $\mu\text{m}$  thick film and the first and second derivatives of the profile. The maximum and minimum of the first derivative, and the zero crossings of the second derivative, delimit the positions of the sample surface. The first derivative also gives the PSF.

The derivative method was applied to determine the PSF for the HoloLab instrument (Paper II). A 12  $\mu\text{m}$  thick transparent PET film (sample 5) was depth profiled for the purpose. The first derivative of the data was then calculated (Figure 11). Fitting of a Lorentzian curve to the first derivative gave a FWHM of 4  $\mu\text{m}$  (Paper II), which was lower than the value obtained with the silicon wafer method (5  $\mu\text{m}$ ) (Paper I). The distance between the maximum and the minimum of the first derivative correctly gave the thickness of the film (12  $\mu\text{m}$ ).

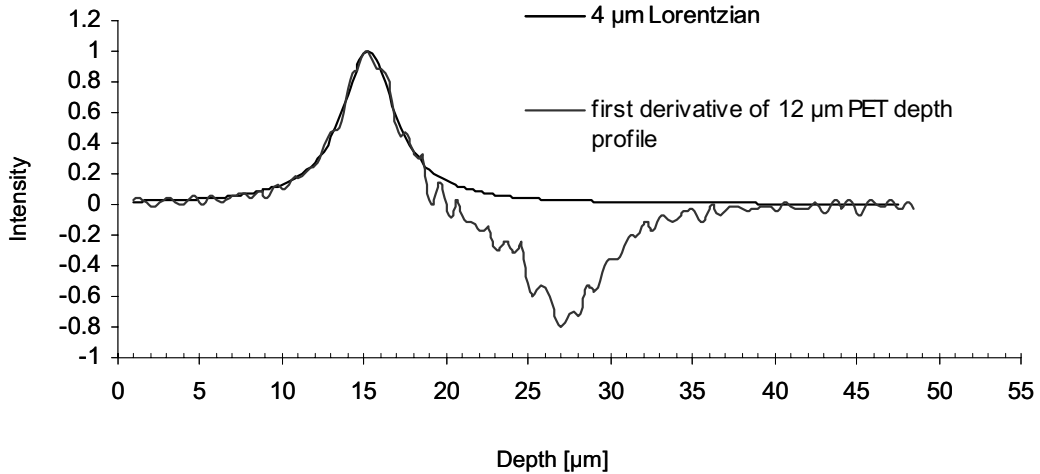


Figure 11. The first derivative of the depth profile of a 12  $\mu\text{m}$  thick PET film gives the PSF of the Raman measurement technique. The derivative is displayed with a fitted Lorentzian curve (FWHM 4  $\mu\text{m}$ ). (Paper II)

### 3.2.4 Layer thickness analysis below the nominal depth resolution

Thin layers were simulated with boxcar functions having thicknesses of 0  $\mu\text{m}$ , 1  $\mu\text{m}$ , 2  $\mu\text{m}$ , 3  $\mu\text{m}$ , 4  $\mu\text{m}$ , 5  $\mu\text{m}$  and 6  $\mu\text{m}$ . A similar convolution with the PSF as above was employed. The zero micrometre thickness was obtained directly by using only the PSF. These layers were produced to determine whether a confocal Raman microscope with nominal depth resolution of 4  $\mu\text{m}$  could be used to determine layer thicknesses less than the nominal depth resolution. Figure 12 illustrates the first derivatives of the simulated depth profiling curves of samples 0  $\mu\text{m}$ , 1  $\mu\text{m}$  and 2  $\mu\text{m}$  thick. Because of the limited depth resolution, the distances between the zero crossings in the second derivative (apparent thickness) were larger than the actual sample thicknesses.

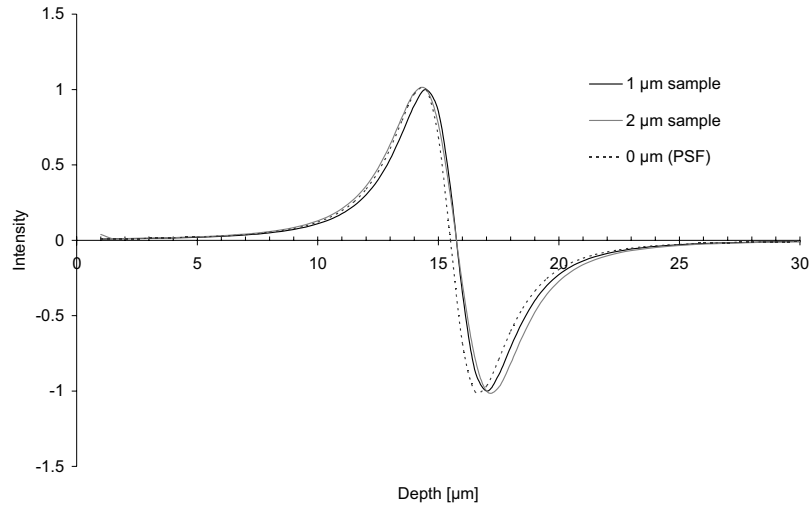


Figure 12. First derivatives of modelled Raman depth profiles of samples 0  $\mu\text{m}$ , 1  $\mu\text{m}$  and 2  $\mu\text{m}$  thick. The distances between the inflection points were larger than the modelled sample thicknesses because of the PSF (FWHM 4  $\mu\text{m}$ ) of the instrument. Apparent thickness values of these thin samples are very close to each other, as can be seen in Figure 13.

Figure 13 shows data extracted from the modelled depth profiling curves. Zero crossings of the second derivatives were used to obtain apparent thickness values. The curve of actual thickness values vs. apparent thickness values approaches the curve  $y = x$ . The difference between these two curves indicates the deviation from the actual thickness values. At 4  $\mu\text{m}$  actual thickness, the difference is small (0.3  $\mu\text{m}$ ) and the result from the second derivative may be used directly. The analysis of layer thicknesses less than 2  $\mu\text{m}$  becomes difficult owing to the steep slope of the curve below that thickness, and the accuracy of the method becomes critical.

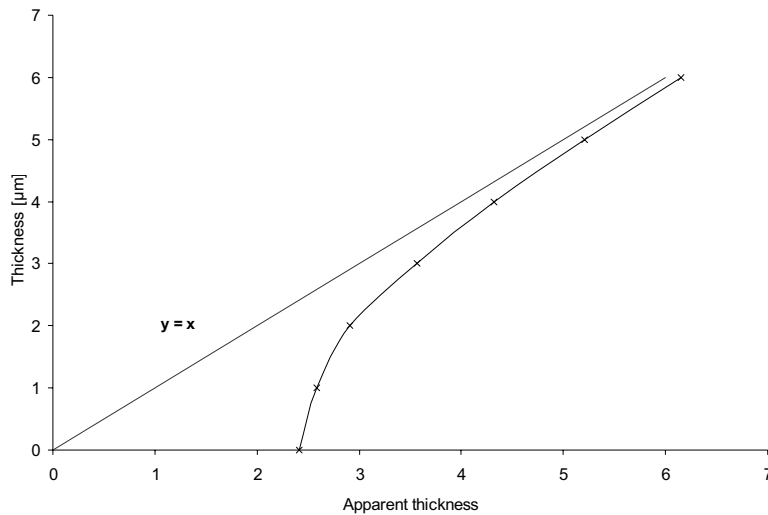


Figure 13. Data calculated from modelled depth profiling data can be used to convert the apparent thickness to actual sample thickness. The distance between the calculated curve and the line that it approaches shows the deviation from the actual thickness.

### 3.2.5 Depth resolution in binder migration studies

The detection of binder migration was studied through model simulation. The PSF (FWHM 4  $\mu\text{m}$ ) was convolved over two separate functions describing the  $\text{CaCO}_3$  and SB-latex concentrations as functions of depth. The simulated  $\text{CaCO}_3$  function showed an even concentration through the 12  $\mu\text{m}$  thickness (boxcar function). In the SB-latex depth profile, the binder migration was simulated by specifying a constant concentration for the first two micrometres and a 20% lower concentration for the rest of the layer (Figure 14). An increasing gradient towards the top surface is evident in the intensity ratio curve, while the differences in the depth profiles are more difficult to observe. The intensity ratio varies by less than 20% because the actual collection volume extends into the physically thicker, lower concentration region, even when the focus is set in the surface. This model simulation illustrates how features that are thinner than the depth resolution are seen with confocal Raman microscopy. In confocal Raman measurements, the sensitivity at the surface is enhanced because the immersion oil filled space above the sample does not give rise to blurring. It can be concluded that the use of surface gradient is useful for the characterization of binder migration, even when the scale of the thickness is less than the nominal depth resolution.

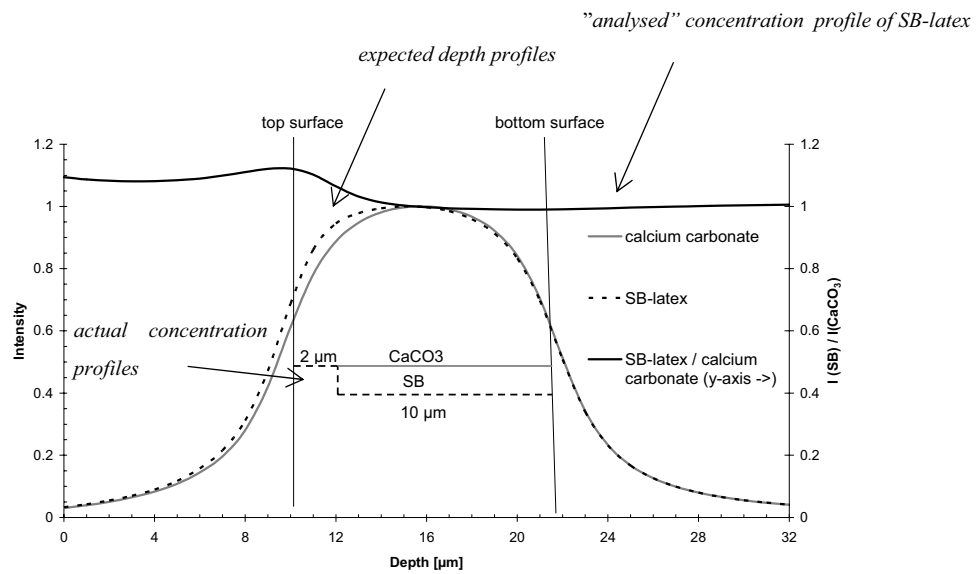


Figure 14. Simulation of detection of binder migration with confocal Raman depth profiling. The  $\text{CaCO}_3$  concentration was set at constant level, while after the surface layer ( $2 \mu\text{m}$ ) the SB-latex content was set 20% lower than the content in the surface layer of the coating. The intensity ratio curve indicates how the migration is observed when the depth resolution is  $4 \mu\text{m}$ . (Paper III)

### 3.3 Spatial resolution in lateral mapping

The lower limit of the lateral resolution in Raman microscopy can be approximated by Abbe's law

$$\div x \approx \frac{\zeta}{2NA}, \quad (3)$$

where  $\zeta$  is the laser wavelength and NA is the numerical aperture of the objective (Schrader 1995). Equation 3 explains how the spatial resolution of Raman microscopy can be altered by selection of the objective. In reality the spatial resolution also depends on the instrument specifications such as the size of the pinhole and on how well the laser beam fills the objective.

The spatial resolution is generally less important in lateral mapping of coated papers than in depth profiling. With the HoloLab Raman microscope the laser spot size with a 10X (NA 0.25) objective was 20  $\mu\text{m}$  and therefore the lateral resolution using the FWHM criterion was approximately 10  $\mu\text{m}$ , while the theoretical limit is at 1.6  $\mu\text{m}$  (eq. 3).

A set of pigment coatings on PET substrate (sample set 9) was used to investigate the depth of sampling for a 10X objective in the case of light scattering paper coatings. Figure 15 illustrates how increase in the coating thickness increases the  $\text{CaCO}_3$  intensity. With change in the light scattering properties of the coating the intensity responses would be altered. Error in the coating thicknesses was considerable in the thinnest coatings. Raman intensities without normalization were also a source of error. However, even though lateral mapping does not provide quantitative information on coating thickness, variation in the coating thickness can be qualitatively mapped together with the chemical composition of the paper coating. Another source of major intensity variation could be the focusing. Our earlier work demonstrated that with a 10X objective the intensity was relatively constant in z-direction in a range of approximately 60  $\mu\text{m}$  (Vyörykkä et al. 2002).

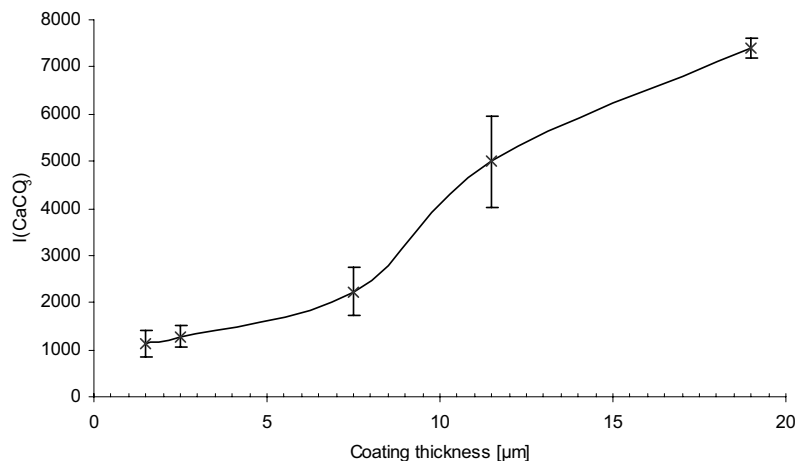


Figure 15. Raman intensity of CaCO<sub>3</sub> and PET as the coating thickness increases. Error bars are given as 95% confidence limits.

In light scattering samples the laser light is diffusely scattered and the diameter is increased, while in transparent samples the focus is sharper and the sample transmits the laser radiation (Schrader 1995). In a strongly light scattering paper coating, laser power reaching the PET substrate is reduced. Moreover, the coating layer restricts backscattered Raman photons from the PET substrate from reaching the detector. The depth sampled with the 10X objective was determined by using the data shown in Figure 15 and the intensities of the PET substrate of the same measurements. Figure 16 presents an exponential decay curve showing a sampling depth of approximately 6 μm in this case.

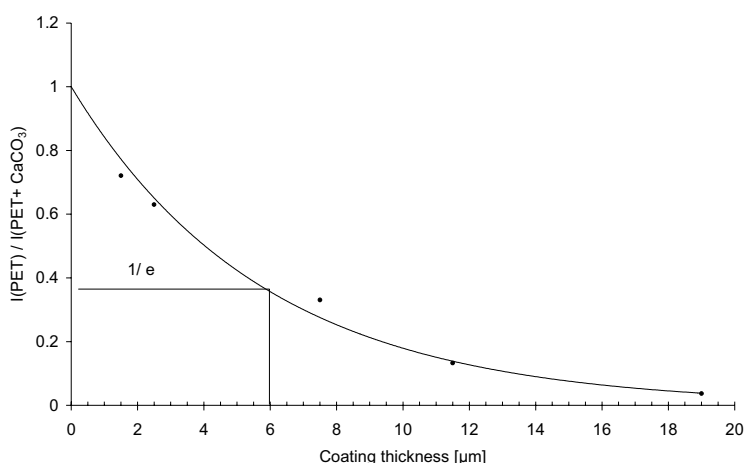


Figure 16. Sampling depth determined with use of coatings of different thicknesses was approximately 6 μm. The PET intensities were normalised to obtain intensity 1 for the zero coating thickness.

For surface sensitive measurements, a metallurgical 100X (NA 0.95) objective with 2.5  $\mu\text{m}$  lateral resolution was employed in the HoloLab Raman instrument. The depth sampled for transparent polymer films with the 100X dry objective was 3  $\mu\text{m}$ . The depth sampled is given as  $1/e$  depth for the PSF half that penetrates into the sample. When the measurement is done from the sample surface, half of the measurement volume described by the PSF is above the sample and does not give rise to a signal. This means that at the surface of a transparent sample the signal is approximately 50% of the maximum. When focusing with the Raman signal, therefore, the maximum signal is achieved deeper inside the sample (see Figure 9). In the case of paper coatings, light penetration is reduced due to light scattering, and focusing with the Raman signal sets the measurement to the surface. The sampling depth using the 100X dry objective is approximated to be 1-2  $\mu\text{m}$ .

### 3.4 Depth profiling of coated and printed papers

Depth profiles of coated and printed papers were measured with an immersion technique that utilizes two refractive index fitted oils (Figure 17). Depth profiling experiments were performed with a 100X oil-immersion objective featuring 4  $\mu\text{m}$  depth resolution, while the lateral resolution was 2.5  $\mu\text{m}$ . The oil between the objective and the cover glass was supplied by the objective manufacturer. The selection of the second oil, which is in contact with the sample, is more critical. This oil should not have any interaction with the sample, or be fluorescent, and it should not have strong Raman bands overlapping with the sample (Paper I). The good depth resolution of Raman microscopes means that, in the case of nonporous materials, interference from the second oil will usually occur only at the surfaces. In pigmented paper coatings, however, the second oil fills the voids at all depths and reduces light scattering markedly. In this work, polydimethylsiloxane with a refractive index of 1.43, was used as the second oil (see Figure 38, Appendix). The refractive indices of common paper coating pigments and binders are approximately 1.55 (Paper I). However, this oil is a major improvement because low refractive index air will be displaced from the coating. The improved depth profiling capability for paper coatings was illustrated in Figure 7 and 8. Details of the performance and benefits of this objective were discussed above and in Paper I.

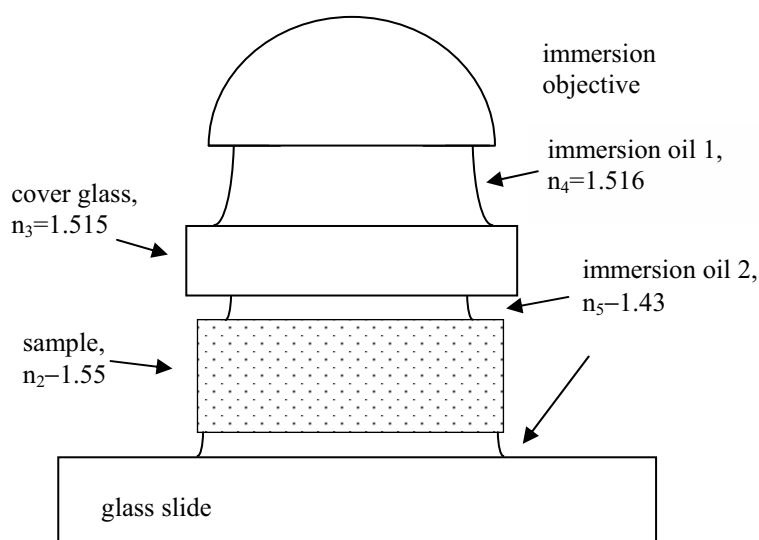


Figure 17. A schematic drawing of the sample preparation for immersion depth profiling (Paper I).

### 3.4.1 Analysis of binder migration

In place of physical cross-sectioning, confocal Raman microscopy provides a possibility for contact-free scanning of cross-sections with the immersion depth profiling method. The cross-section is composed of several depth profiles in a straight line. Figure 18 displays a cross-section map of SB-latex content measured with the immersion depth profiling method (sample 6). The measurement consisted of a line scan of ten depth profiles at 100  $\mu\text{m}$  intervals producing a 0.9-mm-long cross-section of the paper coating.

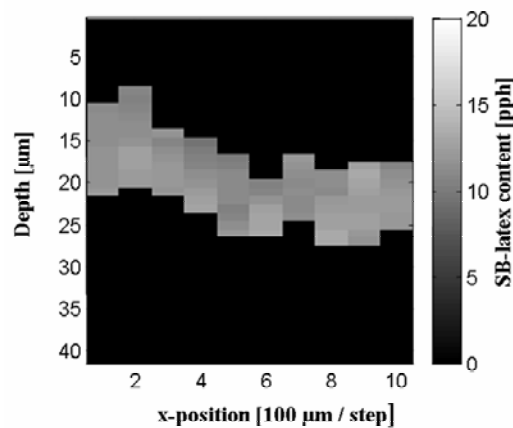


Figure 18. Cross-section image of depth profiled double coated paper giving the SB-latex distribution in the coating cross-section (Paper III).

Table 2 summarizes the findings from the depth profiling data of Figure 18. The average SB-latex content that was detected was equal to the amount applied. Surface content of the latex is an average value of the first layer, while the bottom content of the latex is an average value of the last layer. In this cross-section, the top surface contained less SB-latex than the bottom layer. However, coated papers are still heterogeneous at this scale and more measurements would be required to decide whether or not latex migration has occurred towards the base paper. The uncertainty in the SB-latex content, and thus giving the accuracy of the depth profiling set-up, was determined by measuring ten depth profiles at the same position and calculating the standard deviation of the data.

Table 2. Results from the cross-section depth profiling experiment displayed in Figure 18 (Paper III).

	Analysed value
Average thickness [ $\mu\text{m}$ ]	9 $\mu\text{m}$
Average SB-latex content [pph]	12.0 ( $\pm 0.2$ )
SB-latex content at the surface [pph]	11.3 ( $\pm 0.2$ )
SB-latex content at the bottom [pph]	12.6 ( $\pm 0.2$ )

### 3.4.2 Coating thickness analysis

The thickness profile of double coated samples (sample set 8) having aragonite PCC in the top coating and calcite PCC in the precoating could be determined from the characteristic Raman bands of the allomorphs of  $\text{CaCO}_3$  (calcite  $278\text{ cm}^{-1}$ , aragonite  $208\text{ cm}^{-1}$ ) (see Appendix, Figure 32). In a similar way, thickness profiles were determined for double coated samples in which the two layers could be distinguished by the characteristic bands of  $\text{TiO}_2$  (see Appendix, Figure 34)

Figure 19 and 20 depict the measured thickness profiles of double coated papers (sample set 8) for which 12 depth profiles were measured at  $40\text{ }\mu\text{m}$  distances. The base stock elevation was determined as the bottom surface of the precoating because of the weakness of the Raman signal from the base paper. At certain points, coating penetration into the base paper made it difficult to determine the bottom surface. Independent of the precoating method (blade or MSP), a clear “valley” filling was observed in the top coat application.

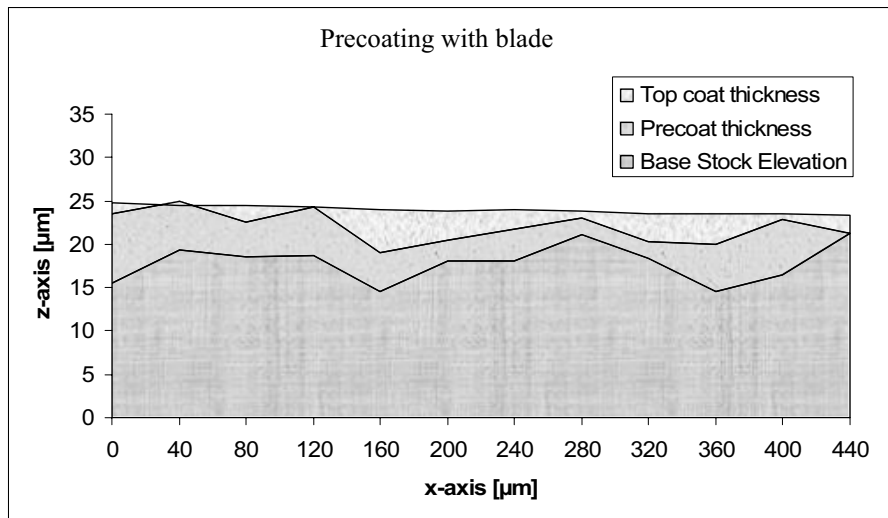


Figure 19. Thickness profiles of a double coated paper where both the pre- and top coatings were applied with a blade coater. The layers could be distinguished by the different Raman bands emerging from calcite (precoating) and aragonite (top coating).

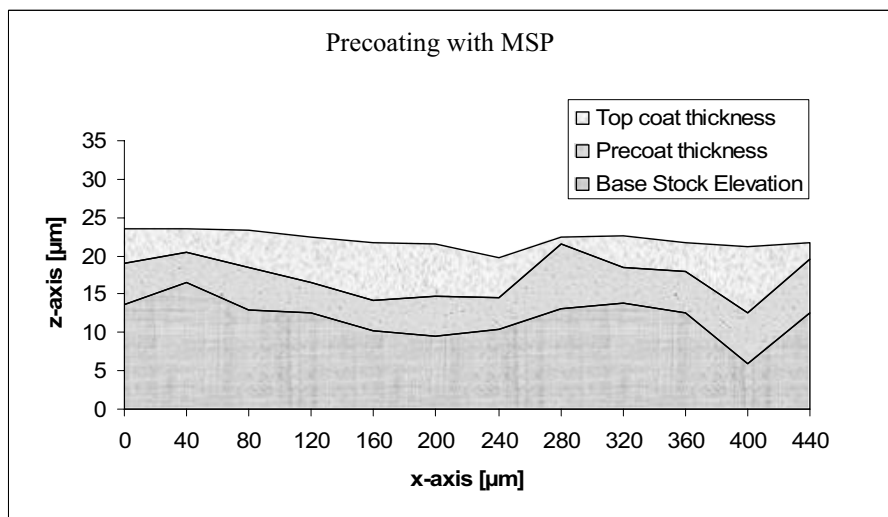


Figure 20. Thickness profiles of a double coated paper where the precoating was applied with MSP and the top coating with a blade coater. The layers could be distinguished by the different Raman bands emerging from calcite (precoating) and aragonite (top coating).

A statistical analysis of the differences between the two precoating methods was made on the basis of 26 depth profiles of each of the four samples (Table 3). The values obtained indicate that more uniform precoating thickness profiles were produced with MSP than with the blade coater. Thus, a more contour-like coating was achieved with the MSP coating method, in accordance with common understanding (Rautiainen and Lehtinen 2000) and recent scientific publications (Hedman et al. 2003, Donigian and Vyörykkä 2004).

Table 3. Statistical data on thickness values for double coated papers (26 thickness values for each sample). A: calcite in precoating, B: TiO<sub>2</sub> and calcite in precoating.

	Sample set 8 A / Blade	Sample set 8 B / Blade	Sample set 8 A / MSP	Sample set 8 B / MSP
Precoat thickness [ $\mu\text{m}$ ]	5.4	4.9	4.8	4.7
Stdev [ $\mu\text{m}$ ]	4.1	3.1	1.9	2.1
Top coat thickness [ $\mu\text{m}$ ]	4.5	4.7	5.4	5.3
Stdev [ $\mu\text{m}$ ]	2.2	2.9	1.4	3.3

### 3.4.3 Determination of ink layer thickness

Figure 21 demonstrates depth profiles of an offset printed paper (sample 7 B) measured from a magenta ink test area. It is also possible to collect Raman spectra through yellow inks. Black and cyan inks, in contrast, are difficult to analyse owing to their strong light absorption at the laser wavelength (785 nm), fluorescing of the dyes and possible burning of the samples under the intense laser beam. Depth profiling through a print allows direct analysis of the SB-latex content under the print and especially under printing defects. Depth profiling through print also gives information about ink pigment, but the oils, binders and other additives commonly used in offset inks cannot be detected.

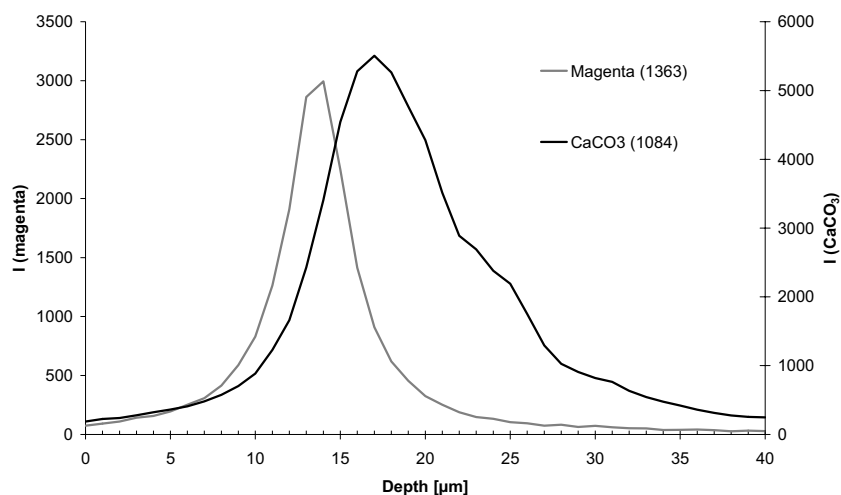


Figure 21. Depth profiles of magenta dye and the CaCO<sub>3</sub> pigment of coated and printed paper (Paper III).

The apparent surface positions of the ink layer and the top of the coating were determined as the zero crossings of the second derivatives of the depth profiles (Figure 22). The second derivative of the coating depth profile had a lot of noise in the back side due to coating penetration into the base paper, which blurred the position of the back surface. Because of the noise in the second derivative the surface positions were confirmed with use of the first derivative, which contained less noise.

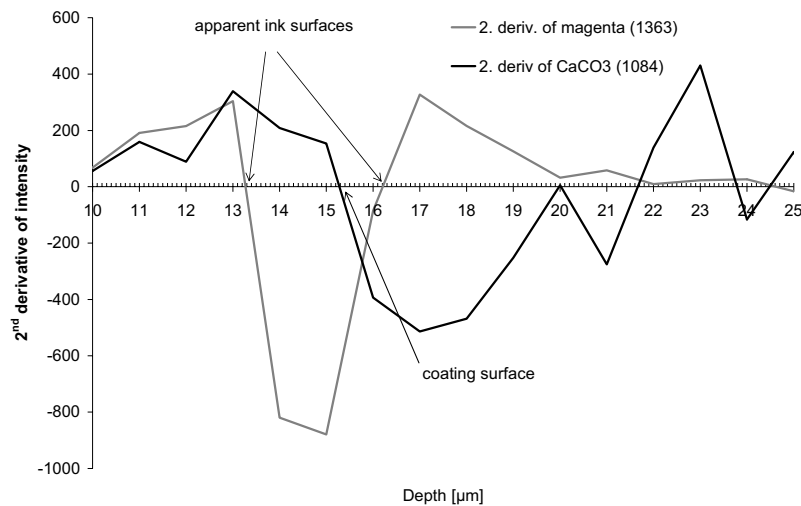


Figure 22. Second derivative of the Raman depth profiles illustrated in Figure 21. The second derivative of the coating back side is noisier due to coating penetration. The x-axis is shifted 1 micrometre towards larger values when compared to the x-axis of the depth profile (Figure 21). (Paper III)

In this single depth profile, the apparent thickness of the ink layer was  $2.9 \mu\text{m}$  corresponding to an actual thickness of  $2.0 \mu\text{m}$  (see Figure 13). The actual thickness value is higher than the typical thickness of offset printed wet ink films ( $1 \mu\text{m}$ ) given by Lepoutre (1989), perhaps because the depth resolution is not sufficient to allow accurate analysis at thicknesses less than  $2 \mu\text{m}$  (see Figure 13). The use of the second derivative allowed analysis of the ink pigment penetration into the coating layer. The definition of ink pigment penetration is technically relatively easy due to the well-defined ink layer and coating surface. Definition of the coating back surface is sometimes more difficult due to coating penetration into the base paper. The penetration of the ink can be calculated through an analysis of the positions of the surfaces of the ink and the coating. It can be assumed that the confocal Raman method broadens the data of these thin layers symmetrically. Thus when the total broadening was reduced by  $0.9 \mu\text{m}$  (difference between apparent thickness and actual thickness), the top surface of the ink was located at  $13.8 \mu\text{m}$ , while the bottom surface was at  $15.7 \mu\text{m}$  (in the depth profile figure the positions are 1 micrometre towards lower values). Since the top

surface of the coating was located at position 15.3  $\mu\text{m}$ , the ink penetration into the coating layer was 0.4  $\mu\text{m}$ .

Uncertainty in the surface position values was reduced by averaging data from several measurements. The uncertainty of an average is inversely proportional to the square root of the number of averaged points. Twenty depth profiles each were measured from samples A and B of sample set 7 and the data were analysed for ink layer thicknesses, ink penetration and SB-latex migration. The analysis of SB-latex migration was based on the gradient (see Figure 14 and related text) to determine if mottling was due to surface content of the SB-latex.

The analysed data are collected in Table 4. Sample A exhibited a larger negative SB-latex gradient signifying greater binder migration towards the coating surface; however, the large error limits indicate very high variation in the gradient for both samples. Moreover, the surface SB-latex values were fairly similar and it may be concluded that there was no consistent difference in the SB-latex migration of the samples. Significant differences were observed in the ink layer values: sample B had a thicker ink layer than sample A. The ink layer thicknesses were also greater than expected. In offset printing the transferred ink layer thickness is typically 1  $\mu\text{m}$  (Lepoutre 1989, Kishida et al. 2001). Sample B also exhibited greater ink penetration into the coating than sample A. In the case of highly porous coatings, the ink can be expected to penetrate totally into the coating (Kishida et al. 2001), but common understanding is that in the standard coated paper grades used in offset printing larger ink pigments and binders remain mostly on the paper surface, while ink oils partially separate and penetrate into the coating structure (Wallström 1991, Ström et al. 2001, Rousu 2002).

In confocal Raman results, insufficient depth resolution limits the conversion from the apparent ink layer thickness to the actual ink layer thickness when thicknesses are less than 2  $\mu\text{m}$ . However, the thicker ink layer of sample B should not yet be below this resolution limit. The conversion affects both top and bottom ink layer surface positions but, owing to the thickness of the coating layer, not the position of the coating surface. A difference in the converted ink layer thickness would also change the ink penetration value. Comparison of the ink layer thicknesses of the samples was nevertheless possible.

Table 4. Results for samples A and B (sample set 7).

Sample set 7	A	B
Apparent ink layer thickness	2.8 ( $\pm 0.2$ )	3.5 ( $\pm 0.3$ )
Ink layer thickness [ $\mu\text{m}$ ]	1.8 ( $\pm 0.3$ )	2.8 ( $\pm 0.4$ )
Ink penetration [ $\mu\text{m}$ ]	0.9 ( $\pm 0.2$ )	1.4 ( $\pm 0.3$ )
SB-latex content at the surface [pph] <sup>1</sup>	15.9 ( $\pm 0.7$ )	15.6 ( $\pm 1.2$ )
SB-latex gradient [pph/ $\mu\text{m}$ ]	-0.003 ( $\pm 0.006$ )	-0.001 ( $\pm 0.004$ )

<sup>1</sup> calibration coefficient 94.3 from paper I was employed. It may not be correct in this case owing to the different coating recipe.

SEM method has usually been applied in coating and ink thickness analysis (Allem 1998, Kishida et al. 2001, Chinga 2002). The SEM method can provide resolution as high as 0.02  $\mu\text{m}/\text{pixel}$ , but prior cross-section preparation and staining are essential for SB-latex analysis in depth direction (Chinga 2002). In high resolution imaging, SEM method is better than confocal Raman depth profiling, but quantification is more reliable with Raman method.

The ink thickness data of confocal Raman data is provided simultaneously with the depth profiling curves of paper coating, which means that SB-latex data and coating thickness data can be correlated with ink film thickness. The analysis of thin layers with confocal Raman depth profiling method may find even better applications in other fields.

### 3.5 Lateral analysis of paper coatings

Chemical mapping with Raman microscopy has been applied to various samples: diamond-like coatings, polymers, optical fibres, biological samples and pharmaceuticals (Hayward et al. 1995, Markwort and Kip 1996, Sijtsema et al. 1998, Clarke et al. 2001). Lateral mapping with confocal Raman microscopy was introduced for paper coatings in 2002 (He et al. 2002, Vyörykkä et al. 2002). However, the areas of the maps have typically been smaller than the unit size of non-uniformity in mottling ( $1 \text{ mm}^2 - 9 \text{ mm}^2$ ; Arai et al. 1988).

#### 3.5.1 Surface mapping of paper coatings

Surface mapping of small areas ( $200 \text{ }\mu\text{m} \times 1000 \text{ }\mu\text{m}$ ) of paper coatings was carried out with the RM 1000 Raman microscope using a 50X objective. Because of the fairly broad focus of the 50X objective (FWHM =  $6 \text{ }\mu\text{m}$ ), the system was not very sensitive to micrometre scale changes in the sample surface position. In general, it was possible to scan  $200\text{-}\mu\text{m}$  lines automatically without refocusing. In light scattering coatings, the set-up allows a sampling depth of approximately  $2\text{-}3 \text{ }\mu\text{m}$ . In total, 200 Raman spectra each were measured from areas of high and low ink density. A microscopy image of the sample is presented in Figure 23 (sample 13). The actual measurement was made over a wider range than shown; the total area was approximately  $200 \text{ }\mu\text{m} \times 1000 \text{ }\mu\text{m}$ . Area averaging was done after the measurements by averaging the SB-latex:CaCO<sub>3</sub> band height ratios.

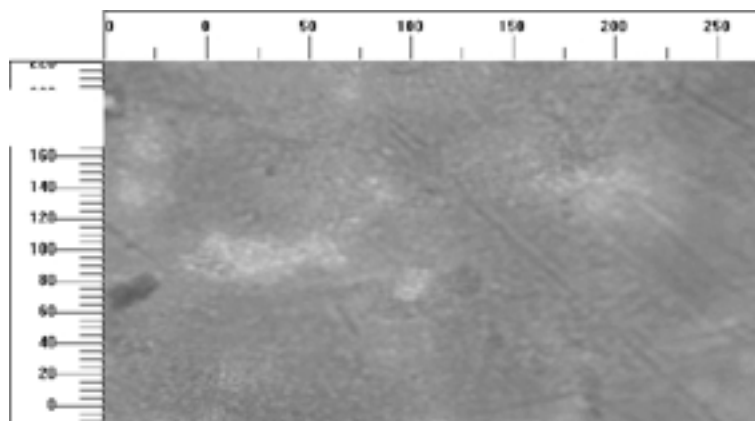


Figure 23. Light microscopy image of a printed paper with strong mottle. 400 Raman spectra were measured ( $200 \times 2$ ) from areas of high and low ink density.

The values for the Raman measurement done in areas of low and high ink density areas are presented in Table 5. The SB-latex variation in small area was obtained as the standard deviation of the 200 SB-latex:CaCO<sub>3</sub> values. The large area variation for the SB-latex was obtained from the same data by averaging the results of 20 successive Raman spectra and calculating the standard deviation of the 10 average values. SB-latex:CaCO<sub>3</sub> band height ratios were similar for the two ink density areas, indicating similar SB-latex surface content. Likewise, the observed values of SB-latex variation were relatively close in the low and high ink density areas, though the variation was less for the high ink density areas in both large and small scales. These results are in agreement with Xiang et al. (2000), who analysed the same sample by LIPS, ESEM and SEM-EDS. They did not observe any difference in chemical structure between this mottled sample and a good sample.

Table 5. SB-latex results for areas of high and low ink density.

	High ink density area	Low ink density area
SB-latex:CaCO <sub>3</sub> ratio x 40	15.8	15.8
SB-latex variation in large area [%]	1.4	1.8
SB-latex variation in small area [%]	7.0	8.8

The HoloLab Raman instrument with a 100X (NA 0.95) objective was used for the collection of surface maps containing many 1 mm<sup>2</sup> squares. The acquisition time for a single Raman spectrum was 20 s. The microscopic area of each measurement spot was enlarged through a computer controlled movement of the sample. During collection of the spectrum the sample was moved under the laser beam in a controlled way (Figure 24) so that the measurement area was increased while the depth sampled was maintained. The speed of the movement was 110 µm/s.

The intensity of the Raman scattering drops drastically with a 100X (NA 0.95) objective if the sample moves out of focus (see Figure 7). An autofocus was programmed to compensate the roughness of the paper samples. The autofocus function employed successive 1 s Raman measurements and monitoring of the peak height of CaCO<sub>3</sub> (1084 cm<sup>-1</sup>) at each vertical position. The focusing was performed in two stages: first coarse focusing with 5 µm step size and then fine focusing with 1 µm step size.

The programmed measurement scheme for surface mapping with the HoloLab Raman instrument is depicted in Figure 24. In this measurement scheme, 1 mm<sup>2</sup> squares are covered completely, while bigger steps of 0.9 cm are employed between the 1 mm<sup>2</sup> squares to cover the larger area of a sheet. This measurement scheme made it possible to observe SB-latex variation in both small and in large scales.

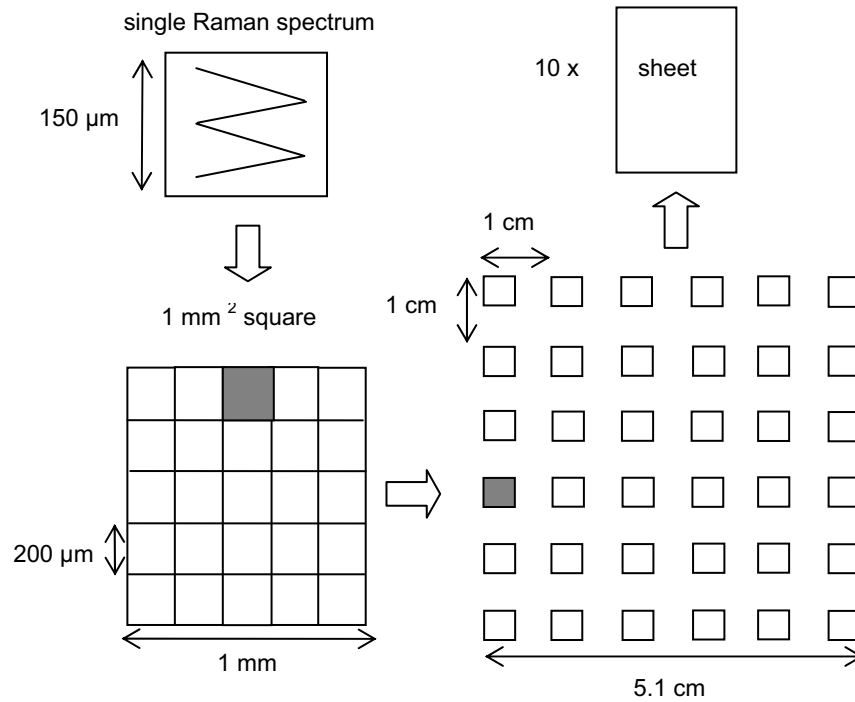


Figure 24. Surface mapping scheme for the HoloLab Raman microscope with 100X objective.

In the surface mapping experiments (see Figure 24), mean and standard deviations were calculated for each 1 mm<sup>2</sup> square from the raw SB-latex:CaCO<sub>3</sub> band height ratios. Small area (150 µm x 150 µm) variation was calculated as the mean of the standard deviations of the measured 1 mm<sup>2</sup> squares. Small area variation can be described as

$$D_S = \text{Average}[\text{Stdev}(x_1), \text{Stdev}(x_2) \dots \text{Stdev}(x_{36})], \quad (1)$$

where  $x_1 - x_{36}$  values represent a set of ratio values inside each 1 mm<sup>2</sup> square. *Stdev* and *Average* are functions of Microsoft Excel. Large area variation was obtained by calculating the standard deviation of the determined mean ratio values of the 1 mm<sup>2</sup> squares. Large area deviation describes the variation in 1 mm<sup>2</sup> areas. It can be written as

$$D_L = \text{Stdev}[\text{Average}(x_1), \text{Average}(x_2) \dots \text{Average}(x_{36})], \quad (2)$$

where  $x_1 - x_{36}$  values represent a set of ratio values inside each  $1 \text{ mm}^2$  square and *Stdev* and *Average* are functions of Microsoft Excel as above. Finally, three values were obtained for each sample: mean ratio, small area variation and large area variation.

With the HoloLab Raman microscope coating surface analysis was carried out for samples differing in pigment size distribution (samples 14 & 15). Twenty-five Raman spectra were measured from each of 36 areas of  $1 \text{ mm}^2$  squares in a single sheet. Altogether 10 sheets were measured, and the total number of Raman spectra was 9000. The results for the samples are given in Table 6. Since sample 14 had coarser pigment (HC60) than sample 15 (Setacarb) the difference in mean ratio values for the two samples may mainly derive from the difference in pigment type. The results presented in Table 1 (sect. 3.1) support this interpretation. Without calibration it is impossible to determine whether there is a difference in the latex content. Both the small and the large area variation values were clearly different indicating a more homogeneous SB-latex –  $\text{CaCO}_3$  distribution for sample 15.

The number of the  $1 \text{ mm}^2$  squares was decreased from 360 to nine (three each in three sheets) to determine if the number of measurements could be decreased. The change in the accuracy of the SB-latex quantification when the number of measurements was decreased is indicated by the 95% confidence intervals (Table 6). According to the results, three  $1 \text{ mm}^2$  squares measured in each of three sheets seem to be enough to determine the SB-latex content of these samples. Large area variation may be sensitive to the sample heterogeneity if only nine mean values are used in the analysis.

Table 6. Surface mapping results for samples 14 and 15 differing in pigment size (Paper IV).

	36 squares of 1mm <sup>2</sup> 10 sheets	3 squares of 1 mm <sup>2</sup> 3 sheets
Mean of SB-latex:CaCO <sub>3</sub> ratio x 100 Sample 14 / 15	9.5 / 13.0	9.6 / 13.2
95% confidence interval for mean Sample 14 / 15	0.02 / 0.02	0.13 / 0.12
SB-latex variation in 150 μm x 150 μm area [%] Sample 14 / 15	9.8 / 6.5	10.2 / 6.9
SB-latex variation in 1 mm <sup>2</sup> [%] Sample 14 / 15	5.1 / 1.9	4.5 / 1.6

### 3.5.2 Imaging of light scattering and reflection

Normally white light consists of waves that vibrate equally in all directions perpendicular to its direction of propagation. Light passing through a polarizer is modified so that the vibration is parallel to the direction of the polarising material. If a polarizer and an analyser are aligned 90° (i.e. crossed polars) to each other, no light will be detected under normal conditions. In optical microscopy, polarizers and analysers are traditionally applied for the analysis of strain and birefringence, while Raman spectroscopy combined with these techniques makes it possible to identify the chemical composition and crystallinity of different areas (Louden 1989). Crossed polars reveal birefringence in colours or extinction varying with the orientation. Distorted strain patterns and birefringence could be invisible under normal conditions. A polarizing microscope was applied in the troubleshooting of coated papers by Quackenbush (1988). In that work, optical and chemical staining were required to identify pigments, binders and foreign materials present in coatings and print. A combination of polarizers or other microscopic techniques with Raman microscopy allows determination of the chemical or structural differences in areas that would otherwise be invisible.

In multiple light scattering, linearly polarized light becomes depolarized. Completely random polarization is observed in samples exhibiting strong multiple light scattering (Stepanek 1993). Thus, the polarization plane of the light is rotated in light scattering. A schematic view

of the set-up for light scattering and reflection imaging is presented in Figure 25. In paper coating applications, crossed polars transmit light, the polarisation plane of which has been rotated  $90^\circ$  due to scattering. Conversely, when a polarizer and an analyser are aligned parallel to each other the contribution of light scattering is reduced and most of the light passing through such a system emerges from specular reflection from the sample surface.

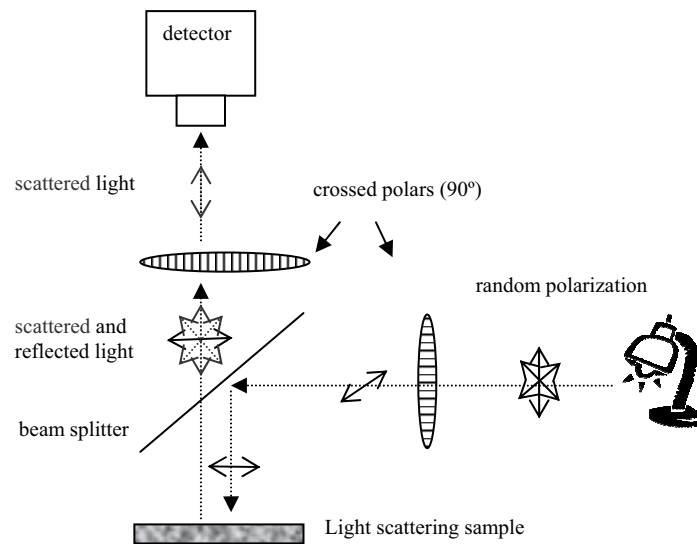


Figure 25. Schematic figure of microscopic light scattering and reflection imaging. Light reflection dominates when the polarizer and analyser are aligned parallel to each other.

Figure 26 displays images acquired with parallel polars. Parallel polars reduce light scattering from the images so that specular reflection is dominant. As can be seen, calendering increases specular reflection, especially in areas where the fibres are close to the surface.

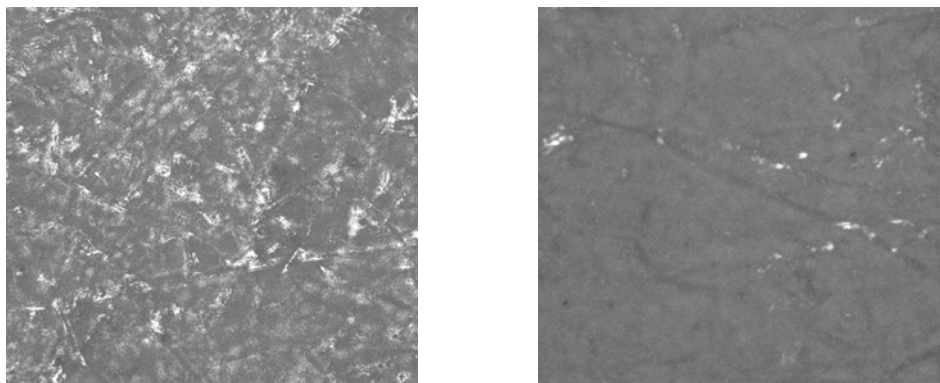


Figure 26. Calendered (left) and uncalendered (right) samples imaged with parallel polars (5X). Brighter areas are seen in the calendered sample. Specular reflection is enhanced with parallel polars. (sample 10, unprinted)

When polars are aligned at 90° to each other, specular reflection is not seen in the image and light scattering is dominant. Crossed polars usually show thinner parts of a paper coating in darker shade (Figure 27). In the case of the printed samples, halftone screening and printed surface interfered in the analysis of the coating and light scattering measurements were performed only for non-printed samples.

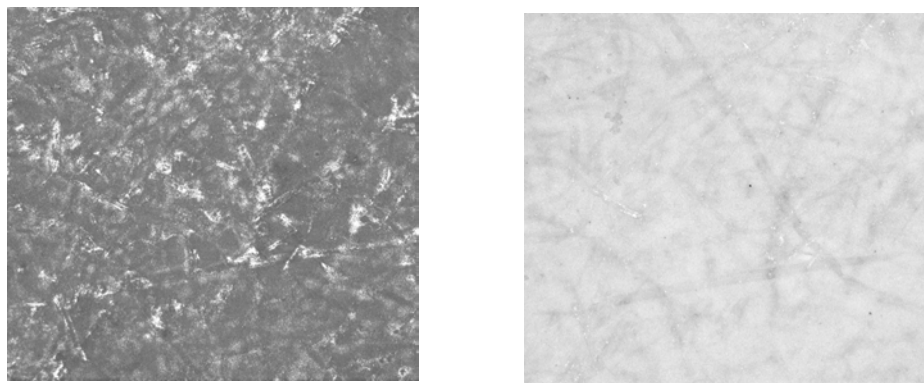


Figure 27. Parallel polar (left) and crossed polar (right) images acquired from the same spot (5X). The fibre network is better seen in the crossed polar image. (sample 10, unprinted)

### 3.5.3 Bulk mapping of paper coatings

Bulk mapping of paper coating was performed with the Hololab Raman instrument using a dry 10X objective. Figure 28 presents Raman maps and a standard light microscopy image of sample 10. The area of the mapping measurement was 390  $\mu\text{m}$  x 390  $\mu\text{m}$  and the step size between the successive measurement points was 10  $\mu\text{m}$ . The total number of Raman measurements was 1521. The sample was printed in a sheet-fed offset press with 40% ink coverage. Simultaneous mapping and imaging provides a way to determine the chemical composition and check the results visually. Several cellulose fibres are evident in the microscope image (Figure 28 a), and are better observed in the Raman intensity map of cellulose (Figure 28 e). Wide variation in intensity is seen in the Raman intensity maps of  $\text{CaCO}_3$  and SB-latex (Figure 28 c & d). Some weak shadowing due to ink can be seen in both maps. However, as the shadowing is the same for latex and  $\text{CaCO}_3$ , it does not have any effect on the SB-latex: $\text{CaCO}_3$  ratio, which was of primary interest in this mapping experiment. Cellulose fibres are more visible in the areas of low intensity of coating components. Hence, these variations together indicate variation in coating thickness. Since calendering reduces porosity and opacity (Suontausta 2002), the coating component intensities may have been somewhat lowered by the reduced light scattering. Ink densities (Figure 28 b) are lower in

areas where cellulose fibres are closer to the surface and the coat weight is lower. The measurement scale was too small to detect visible print mottle. The SB-latex distribution displayed in Figure 28 *f* indicates lower SB-latex content in the low coat weight areas. The base paper may have filtered out the bigger  $\text{CaCO}_3$  pigment particles while allowing part of the smaller latex particles to permeate into the base paper.

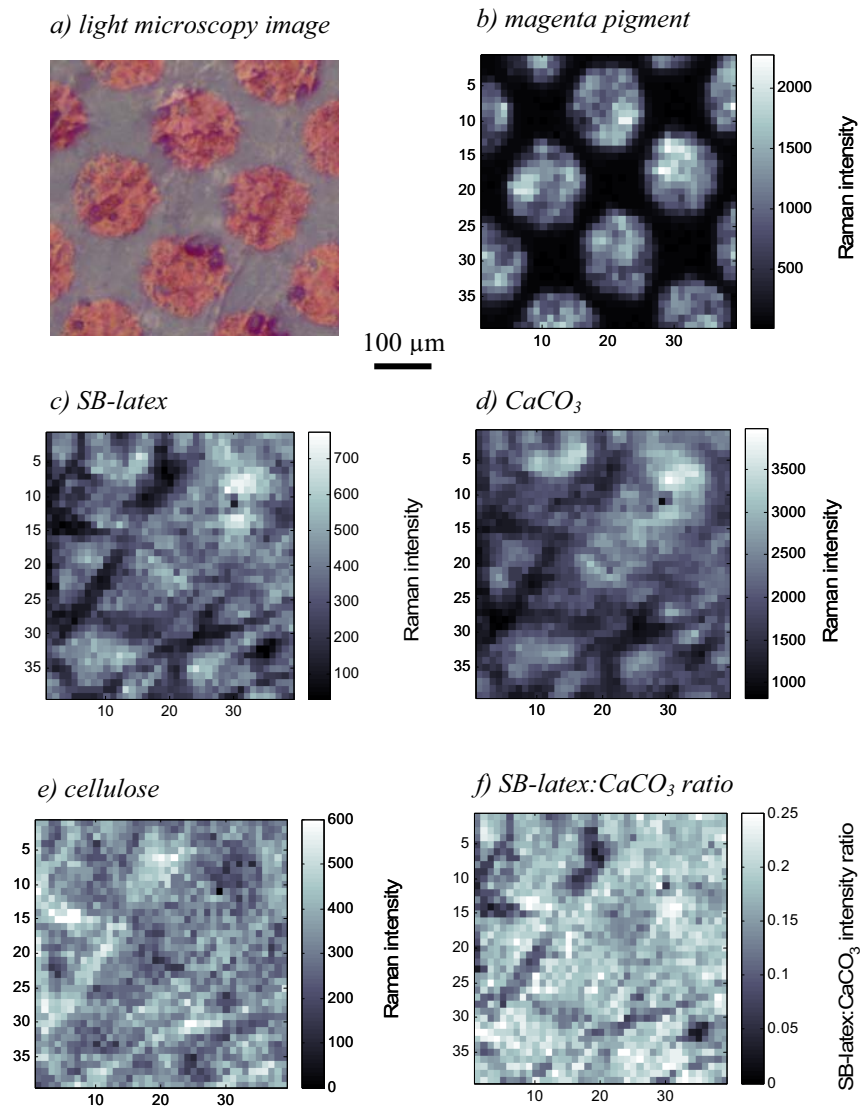


Figure 28. A standard light microscopy image (*a*) and Raman maps (*b-f*) from the same area of a printed sample. The area of mapping was  $390\ \mu\text{m} \times 390\ \mu\text{m}$ . (Paper IV)

Larger areas can be measured within the same analysis time by increasing the step size between the Raman measurements. Increased step size leads to decrease in the spatial resolution. A larger area map was measured for sample A of sample set 7 by increasing the step size to  $50\ \mu\text{m}$ . The total analysed area was  $1.75\ \text{mm} \times 2.25\ \text{mm}$ . As is evident from

Figure 29 *a*, the latex distribution is even, though variations can be seen in areas of low coat weight mostly due to the noise appearing at low Raman intensities. Again, SB-latex and  $\text{CaCO}_3$  (Figure 29 *b-c*) exhibit wide but similar variation in intensity. Cellulose (Figure 29 *d*) shows higher intensities in areas where the coating intensities were lower, indicating variation in coat weight. As before, the coating component intensities may have been somewhat lowered due to calendering. A weak variation is also observed in the magenta ink pigment intensity map (Figure 28 *e*). The magenta intensity map took on a confused appearance in the halftone print as a result of the large step size employed in the mapping.

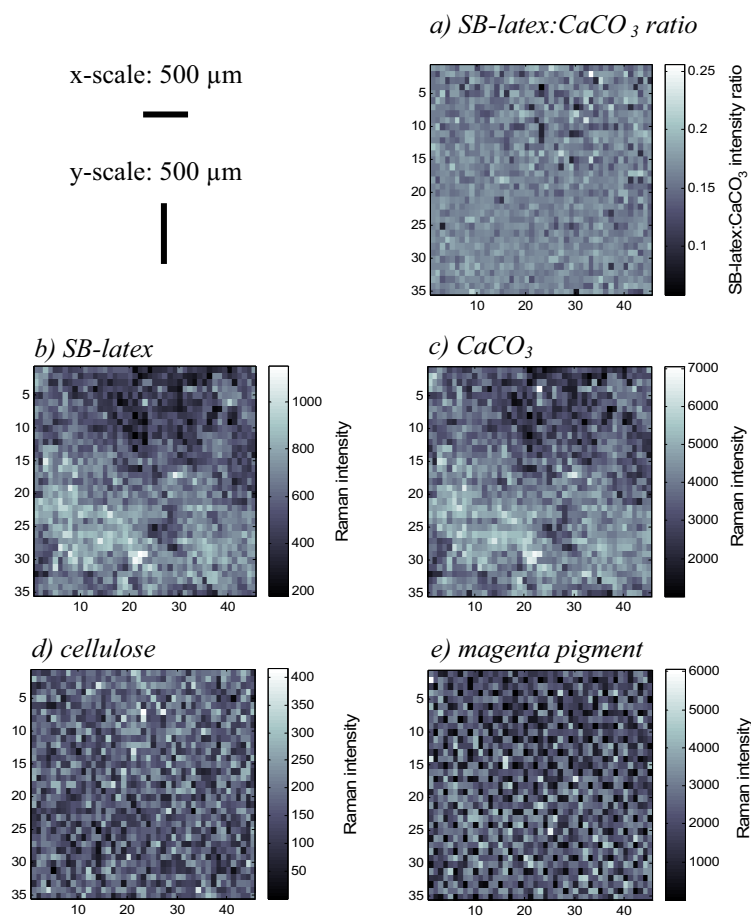


Figure 29. Raman maps of printed paper. The area of the analysis was 1.75 mm x 2.25 mm. (Paper IV)

Figure 30 presents light scattering and reflection images together with Raman maps for sample 12. Microscopy images and Raman maps were taken from the same area (1.75 mm x 2.25 mm). Again, the SB-latex and  $\text{CaCO}_3$  Raman intensity maps display a similar pattern (Figure 30 *c* and *d*). The cellulose Raman intensity map (Figure 30 *e*) shows a complementary image signifying an uneven coat weight distribution, as earlier. Calendering could have

caused some lowering of the coating intensities. In the light scattering image (Figure 30 *a*), cellulose fibres appear as dark areas. A homogeneous dark area indicates lower coat weight, as suggested by the Raman intensity maps of the coating components. The reflection image is more surface sensitive and it rather displays specular reflection from the surface than diffuse scattering. In the reflection image, higher intensities generally appear in the areas where the fibres are at the surface, as illustrated in Figure 26. That is probably due to higher pressure in calendering of the coating in these areas. The SB-latex distribution (Figure 30 *f*) was homogeneous, though some variation was observed in areas of low coat weight.

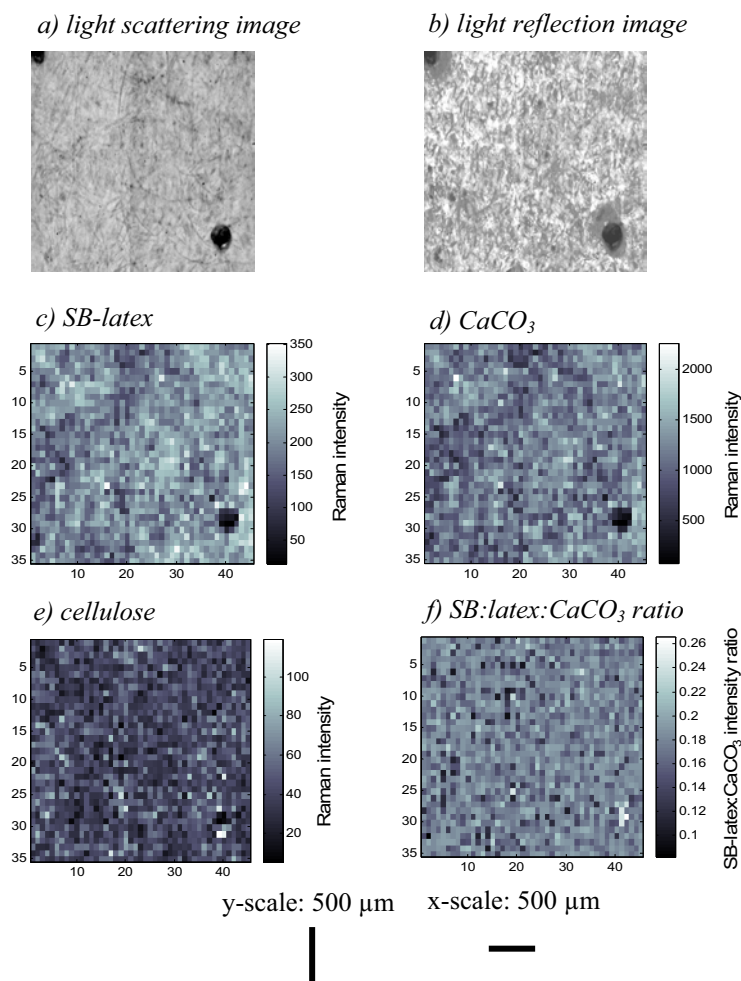


Figure 30. Raman intensity maps of coated paper (*c-f*) and light scattering and reflection images (*a* and *b*) of sample 12 acquired with a polarizer and an analyser in a light microscope. The area of the microscopy images and Raman mapping was 1.75 mm x 2.25 mm. To cover the same area, the microscopy images were stitched together from four separate images. The dark spots in the images are pinhole marks.

### **3.6 Limitations of Raman microscopy in paper coating analysis**

One of the greatest limitations of Raman spectroscopy is that molecules with only weakly polarizable bonds produce an inherently weak Raman spectrum. Thus, coating components such as polyvinyl acetate (PVAc) latices and starches are difficult to detect in paper coatings in their normal concentrations. PVAc could not be detected when the content was 12 pph, even when the acquisition time was increased to several minutes. Typical coatings of light weight coated (LWC) paper contain only 4-8 pph of starch (Bruun 2000) and starch may be even more difficult to detect. This work focused on SB-latex, which is easily detected in paper coatings. In some cases, particularly with certain kaolin grades and inks, fluorescence may limit the detection of signals or prevent Raman analysis. In immersion depth profiling, polydimethylsiloxane oil quenched the fluorescence and it was a less of a problem in immersion measurements than in dry measurements. Typically, coatings containing 80 pph kaolin and even coatings with 100 pph of kaolin were measured with dry optics.

Limited depth resolution may reduce the accuracy of the analysis, especially in the analysis of an ink layer or the analysis of the first micrometre. Microtome cross-sectioning with lateral scanning over the cross-section provides better depth resolution. Use of lateral resolution, which is roughly half of the depth resolution, improves the accuracy. However, the preparation of cross-sections is time consuming. The small size of the measurement area is a limiting factor in the analysis of heterogeneous paper coatings. The small spot size means that quantitative analysis by depth profiling method is time consuming, which is one reason why more attention was paid later to the lateral mapping of coatings.

## 4 Conclusions

Confocal Raman microscopy has been shown to be a beneficial tool in paper coating analysis. Sample preparation is minimal and the data analysis was established during the work. Raman measurements were performed in two modes: depth profiling and lateral mapping.

Raman detects the following chemicals typically applied in paper coating: CaCO<sub>3</sub> (aragonite / calcite), kaolin (fluorescence may interfere), TiO<sub>2</sub> (anastase / rutile), gypsum, talc and SB-latex or other styrene-based lattices (see Raman spectra in the Appendix). In addition, magenta, yellow and cyan offset printing inks can usually be measured. In depth profiling, cyan printed areas absorb the laser light (785 nm) and limit the depth sampled.

Calibration was observed to depend on the pigment type as well as on the pigment mixture applied in the coating. Moreover, the SB-latex:CaCO<sub>3</sub> band height ratio changed with the T<sub>g</sub> value of the SB-latex, as expected. It is always better, to produce a set of calibration samples containing the same chemicals as in the coating. If the coating recipes are similar a semi-quantitative comparison of SB-latex contents is possible without calibration. As an example, if the applied SB-latex content was 10 pph, 10% change in the SB-latex:CaCO<sub>3</sub> band height ratio would correspond to a change of 0.1 pph. This kind of internal comparison may be beneficial in quality control or in monitoring the effect of changed process conditions when the coating recipe is kept similar.

One of the major achievements in this work was the development of an immersion technique for confocal Raman depth profiling and its application to coated papers. At the time of development, the immersion technique was not applied in the field of confocal Raman microscopy. Moreover, depth profiling is more challenging for strongly light scattering paper coatings than the transparent polymer films more usually investigated by Raman microscopy. The benefits of the immersion technique for depth profiling are considerable. The immersion technique provides better depth resolution, and focusing depth is the same as the measurement depth. Moreover, owing to light scattering, depth profiling of paper coatings would be impossible without wetting the sample.

Depth profiling can be applied to investigations of SB-latex migration. Measurement can be done under printing defects and the results can be correlated with coat weight variation, since thickness information is always present in depth profiling data. Thicknesses seem to be somewhat overestimated in the ink layer analysis, but relative differences can be assigned and compared. The differences observed in calcite and aragonite Raman spectra allowed separate thickness profile analysis of the precoating and top coating.

No sample preparation is needed in lateral mapping. Lateral mapping provides access to various probe depths, giving information about the coating surface or the bulk coating. Lateral mapping enables measurements of larger areas in a shorter time than depth profiling.

Surface mapping of SB-latex and SB-latex variation in different scales is useful for coating surface analysis, since ink-coating interaction takes place at the surface. In the surface analysis, measurement of relatively large areas was achieved and a method for latex content and its variation in different scales was developed. In principle, bulk and surface mapping can be performed from the same area successively and the information from different depths can be compared.

Lateral mapping of the bulk coating gives information on the SB-latex content, and the information can be combined with coat weight and print density variation. Through lateral mapping, therefore, it is possible to correlate printing defects with the distribution of coating chemicals and the coat weight distribution. Moreover, with Raman microscopy all the light microscopy accessories can be employed and the information obtained can be combined without taking the sample out of the sample stage.

Results presented in this doctoral thesis provide evidence that confocal Raman microscopy is a powerful tool for characterization of the chemical and physical composition of printed and coated papers. The technique provides quantitative information on SB-latex in the x-y-z direction and it can usefully be applied in SB-latex migration analysis, as was the aim of this method development.

## 5 Literature

Agarwal, U.P. and Atalla, R.H., Raman spectroscopy, in T.E. Connors and S. Banerjee, ed., Surface analysis of paper, CRC, 1995, p. 152

Allem, R., Characterization of paper coatings by scanning electron microscopy and image analysis, Journal of Pulp and Paper Science, 24(10), 1998, p. 329

Arai, T., Yamasaki, T., Suzuki, K., Ogura, T. and Sakai, Y., The relationship between print mottle and coating structure, Tappi Journal, 71(5), 1988, p. 47

Aspnes, D.E. and Studna, A.A., Dielectric functions and optical parameters so Si, Ge, GaP, GaAs, GaSb, InP, InAs from 1.5 to 6.0 eV, Physical Review B, 27(2), 1983, p. 985

Baia, L., Gigant, K., Posset, U., Petry, R., Schottner, G., Kiefer, W. and Popp, J., Confocal Raman investigations on hybrid polymer coatings, Vibrational Spectroscopy, 29(1-2), 2002, p. 245

Baldwin, K.J. and Batchelder, D.N., Confocal Raman microspectroscopy through a planar interface, Applied Spectroscopy, 55(5), 2001, p. 517

Bauer, C., Amram, B., Agnely, M., Charmot, D., Sawatzki, J., Dupuy, N. and Huvenne, J-P., On-line monitoring of a latex emulsion polymerization by fiber-optic FT-Raman Spectroscopy. Part I: Calibration, Applied Spectroscopy, 54(4), 2000, p. 528

Belaroui, F., Grohens, Y., Boyer, H. and Holl, Y., Depth profiling of small molecules in dry latex films by confocal Raman spectroscopy, Polymer, 41(21), 2000, p. 7641

Bitla, S., Tripp, C. and Bousfield, D.W., A Raman spectroscopic study of migration in paper coatings, Journal of Pulp and Paper Science, 29(11), 2003 p. 382

Bougeard, D., Crystals, in B. Schrader, ed., Infrared and Raman spectroscopy, VCH, 1995, p. 314

Bruun, S-E., Starch, in E. Lehtinen, ed., Fapet, 2000, p. 241

Chinga, G., Structural studies on LWC paper coating layers using SEM and image analysis techniques, Academic Dissertation for the Degree of Doctor of Science in Technology, Norwegian University of Science and Technology, Norway, 2002, 108 p.

Clarke, F.C., Jamieson, M.J., Clark, D.A., Hammond, S.V., Jee, R.D. and Moffat, A.C., Chemical image fusion. The synergy of FT-NIR and Raman mapping microscopy to enable a more complete visualization of pharmaceutical formulations, *Analytical Chemistry*, 73(10), 2001, p. 2213

Donigian, D.W. and Vyörykkä, J., Maximizing the ratio of brightness gain to contrast mottle – Part 1, Theory and general recommendations, TAPPI Coating Conference and Trade Fair, Baltimore, MD, United States, May 17-18 2004, in press

Engström, G. and Lafaye, J.F., Precalendering and its effect on paper coating interaction, *Tappi Journal*, 75(8), 1992, p. 117

Engström, G. and Rigdahl, M., Effect of printability and print quality, in M.J. Whalen-Shaw, ed., *Binder migration in paper and paperboard coatings*, Tappi Press, Atlanta, GA, USA, 1993, p. 61

Engström, G., Formation and consolidation of coating layer and the effect on offset-print mottle, *Tappi Journal*, 77(4), 1994, p. 160

Everall, N., Modeling and measuring the effect of refraction on the depth resolution of confocal Raman microscopy, *Applied Spectroscopy*, 54(6), 2000, p. 773

Everall, N., Confocal Raman microscopy: Why the depth resolution and spatial accuracy can be much worse than you think, *Applied Spectroscopy*, 54(10), 2000, p. 1515

Forsström, U., Interactions between base paper and coating color in metered size press coating, Academic Dissertation for the Degree of Doctor of Science in Technology, Helsinki University of Technology, Finland, 2003, 99 p.

Fujiwara, H. and Kline, J.E., Ultraviolet absorption of styrene-butadiene latex on pigment coated paper, Tappi Journal, 70(12), 1987, p. 97

Gagnon, R.E., Parish, T.D. and Bousfield, D.W., A mechanism to explain particle size segregation and binder depletion during coating, Tappi Journal, 84(5), 2001, p. 66

Gane, P.A.C, Mottle and the influence of coating and binder migration, Paper technology, 30(4), 1989, p. 34

Gonzalez, R.C. and Wintz, P., Digital Image Processing, 2<sup>nd</sup> edition, Addison-Wesley Publishing Company, 1987, 503 p.

Govil, A., Pallister, D.M. and Morris, M.D., Three-dimensional digital confocal Raman microscopy, Applied Spectroscopy, 47(1), 1993, p. 75

Griffiths, P.R. and de Haseth, J.A., Fourier transform spectrometry, John Wiley & Sons, 1986, p. 14

Groves, R., Matthews, G.P., Heap, J., McInnes, M.D., Penson, J.E. and Ridgway, C.J., Binder migration in paper coatings – a new perspective, 12<sup>th</sup> Fundamental Research Symposium, proceedings, Oxford, 2003, p. 1149

Guyot, C., Amram, B. and Ubrich, J.M., Raman-microscopic study of mottling of coated paper, Wochenblatt fuer Papierfabrikation, 123 (14/15), 1995, p. 646

Hajadoost, S. and Yarwood, J., Depth profiling of poly(methyl methacrylate), poly(vinyl alcohol) laminates by confocal Raman microspectroscopy, Applied Spectroscopy, 50(5), 1996, p. 558

Hajadoost, S., Olsthoorn, M. and Yarwood, J., Depth profiling study of effect of annealing temperature on polymer/polymer interfaces in laminates using confocal Raman microspectroscopy, *Applied Spectroscopy*, 51(12), 1997, p. 1784

Halttunen, M., Vyörykkä, J., Hortling, B., Tamminen, T., Batchelder, D., Zimmermann, A. and Vuorinen, T., Study of residual lignin in pulp by UV resonance Raman spectroscopy, *Holzforschung*, 55(6), 2001, p. 631

Halttunen, M., Löija M., Vuorinen, T., Stenius, P., Tenhunen, J. and Kenttä, E., Determination of SB-latex distribution at paper coating surfaces with FTIR/ATR spectroscopy, TAPPI Coating Conference and Trade Fair, San Diego, CA, United States, May 6-9 2001, p. 174

Hayward, I.P., Baldwin, K.J., Hunter, D.M., Batchelder, D.N. and Pitt, G., Direct imaging and confocal mapping of diamond films using luminescence and Raman scattering, *Diamond and Related Materials*, 4(5-6), 1995, p. 617

He, P., Bitla, S., Bousfield, D. and Tripp, C., Raman spectroscopic analysis of paper coatings, *Applied Spectroscopy*, 56(9), 2002, p. 1115

Hedman, A., Grön, J. and Rigdahl, M., Coating layer uniformity as affected by base paper characteristics and coating method, *Nordic Pulp and Paper Research Journal*, 18(3), 2003, p. 333

Hendra, P.J., Fourier Transform Raman Spectroscopy, in J.J. Laserna, ed., *Modern techniques in Raman spectroscopy*, John Wiley & Sons, 1996, p 73.

Hird, K.F., *Offset lithographic technology*, the Goodheart-Willcox Company, 1995, 720 p.

Häkkinen, H.J., Development of a method based on laser-induced plasma spectrometry for rapid spatial analysis of material distribution in paper coatings, *Academic Dissertation for the Degree of Doctor of Philosophy*, University of Jyväskylä, 1998, 60 p.

Häkkinen, H.J. and Korppi-Tommola, J.E.I., Analysis of coating structure by laser-induced plasma spectrometry. TAPPI Advanced Coating Fundamentals Symposium, Proceedings, Toronto, Apr. 29-May 1, 1999, p. 191

Kent, H.J., Climpson, N.A., Coggon, L., Hooper, J.J. and Gane, P.A.C., Novel techniques for quantitative characterization of coating structure, Tappi Journal, 69(5), 1986, p. 78

Kenttä, E., Juvonen, K., Halttunen, M. and Vyörykkä, J., Spectroscopic methods for determination of latex content of coating layers, Nordic Pulp and Paper Research Journal, 15(5), 2000, p. 579

Kim, L.H., Pollock, M.J., Wittbrodt, E.L., Roper III, J.E., Smith, D.A., Stolarz, J.W., Rolf, M.J., Green, T.J. and Langolf, B.J., Reduction of back-trap mottle through optimization of the drying process for paper coatings, part I, Tappi Journal, 81(8), 1998, p. 153

Kishida, T., Kouichirou, A., Fukui, T. and Kanou, S., Influence of coating pore structure and ink set property on ink dryback in sheet-fed offset printing, TAPPI Coating Conference and Trade Fair, San Diego, CA, United States, May 6-9 2001, p. 183

Kugge, C., Consolidation and structure of paper coating and fibre systems, Academic Dissertation for the Degree of Doctor of Philosophy, KTH, Stockholm, 2003, 74 p.

Lee, D.I. and Whalen-Shaw, M.J., Fundamentals and strategies, in M.J. Whalen-Shaw, ed., Binder migration in paper and paperboard coatings, Tappi Press, Atlanta, GA, USA, 1993, p. 19

Lee, D.I., Latex, in E. Lehtinen, ed., Fapet, 2000, p. 197

Lehtinen, E., Introduction to pigment coating of paper, in E. Lehtinen, ed., Fapet, 2000, p. 14

Lepoutre, P., The structure of paper coatings: An update, Tappi press, Atlanta, 1989, 56 p.

Lin-Vien, D., Colthup, N.B., Fateley, W.G. and Grasselli, J.G., The handbook of Infrared and Raman characteristic frequencies of organic molecules, Academic press, 1991, 503 p.

Louden, J.D., Raman microscopy, in D.J. Gardiner and P.R. Graves, ed., Practical Raman spectroscopy, Springer-Verlag, 1989, p. 119-151

Markwort, L. and Kip, B., Micro-Raman imaging of heterogeneous polymer systems: General applications and limitations, Journal of Applied Polymer Science, 61, 1996, p. 231

Niemelä, P., Hietala, E., Ollanketo, J., Tornberg, J., Pirttinen, E. and Stenius, P., FT-Raman spectroscopy as a tool for analyzing the composition of recycled paper pulp, Progress in Paper Recycling, 8(4), 1999, p. 15

Oittinen, P. and Saarelma H., Printing, Fapet, 1998, p. 133

Pelletier, M.J., Quantitative analysis using Raman spectrometry, Applied Spectroscopy, 57(1), 2003, p. 20A

Quackenbush, D., Case studies on the use of the optical microscope in the analysis of coated papers, Tappi Journal, 71(5), 1988, p. 70

Rautiainen, P. and Lehtinen, E., Multiple coating of paper, in E. Lehtinen, ed., Fapet, 2000, p. 567

Ranger, A.E., Binder migration during drying of pigment coatings, Paper Technology, 35(10), 1994, p. 40

Reinecke, H., Spells, S., Sacristan, J., Yarwood, J. and Mijangos, C., Confocal Raman depth profiling of surface-modified polymer films: Effects of sample refractive index, Applied Spectroscopy, 55(12), 2001, p. 1660

Rousu, S., Differential absorption of offset ink constituents on coated paper, Academic Dissertation for the Degree of Doctor of Science in Technology, Åbo Akademi University, Finland, 2002, 102 p.

Sacristan, J., Mijangos, C., Reinecke, H., Spells, S. and Yarwood, J., Depth profiling of modified PVS surfaces using confocal Raman microspectroscopy, *Macromolecular Rapid Communications*. 21, 2000, p. 894

Schrader, B., General survey of vibrational spectroscopy, in B. Schrader, ed., *Infrared and Raman spectroscopy*, VCH, 1995, p. 7

Schrader, B., Tools for infrared and Raman spectroscopy, in B. Schrader, ed., *Infrared and Raman spectroscopy*, VCH, 1995, p. 63

Schrof, W. and Häußling, L., Depth resolution of drying processes in UV-curable coatings, *Farbe & Lack*, 103(7), 1997, p. 22

Sijtsema, N.M., Wouters, S.D., De Grauw, C.J, Otto, C. and Greve, J., Confocal direct imaging Raman microscope: Design and applications in biology, *Applied Spectroscopy*, 52(3), 1998, p. 348

Spiekermann, M., Quantitative analysis, automatic quality control, in B. Schrader ed., *Infrared and Raman spectroscopy*, VCH, 1995, p. 411

Stepanek, P., Static and dynamic properties of multiple light scattering, *Journal of Chemical Physics*, 99(9), 1993, p. 6384

Ström, G., Gustafsson, J. and Sjölin, K., Printing papers separation of ink constituents during ink setting on coated surfaces, TAPPI Coating Conference and Trade Fair, San Diego, CA, United States, May 4-5, 2001, p. 269

Sundqvist, H., Structure and CSWO printing press runnability of a matt LWC paper grade – Raman spectroscopic approach, M.Sc. Thesis, Helsinki University of Technology, Finland, 2003, 110 p.

Suontausta, O., Coating and calendering – means of improving surface of coated paper for printing, Academic Dissertation for the Degree of Doctor of Science in Technology, Helsinki University of Technology, Finland, 2002, 177 p.

Tabaksblat, R., Meier, R.J. and Kip, B.J., Confocal Raman microspectroscopy: Theory and application to thin polymer samples, *Applied Spectroscopy*, 46(1), 1992, p. 60

Turrell, G. and Dhamelincourt, P., Micro-Raman spectroscopy, in J.J. Laserna ed., *Modern techniques in Raman spectroscopy*, John Wiley & Sons, 1996, p. 109

Van Gilder, R.L., An investigation of latex particle clustering in the wet coating color, *Tappi Journal*, 3(1), 2004, p. 7

Vikman, K. and Sipi, K., Applicability of FTIR and Raman spectroscopic methods to the study of paper-ink interactions in digital prints. *Journal of Imaging Science Technology*, 47(2), 2003, p. 13

Vyörykkä, J., Halttunen, M., Tenhunen, J. and Iitti, H., Analysing a sample in Raman spectroscopy, FI patent application 19992439, Nov. 12, 1999

Vyörykkä J., Confocal Raman depth profiling in the depth profiling of paper coating colours, M.Sc. Thesis, University of Oulu, Finland, 1999, 69 p.

Vyörykkä, J., Iitti, H., Vuorinen, T. and Stenius, P., Raman microspectroscopy in the lateral mapping of paper coating composition, TAPPI Coating and Graphic Arts conference and Trade Fair, Orlando, USA, 2002, p. 265

Wallström, E., Analytical measurement of the penetration of ink in to paper, SFL konferenssen, 13-15 May, 1991, p. 8:1

Williams, K.P.J., Pitt, G.D., Batchelder, D.N. and Kip, B.J, Confocal Raman microspectroscopy using a stigmatic spectrograph and CCD detector, *Applied Spectroscopy*, 48(3), 1994, p. 232

Wilson, T., Optical aspects of Confocal Microscopy, in T. Wilson, ed., *Confocal microscopy*, Academic press, p. 93

Wilson, T., Confocal Microscopy, in T. Wilson, ed., *Confocal microscopy*, Academic press, p. 1

Xiang, Y., Bousfield, D.W., Hassler, J., Coleman, P. and Osgood A., Measurement of local variation of ink tack dynamics, *Journal of Pulp and Paper Science*, 25(9), 1999, p. 326

Xiang, Y., Bousfield, D.W., Coleman, P. and Osgood, A., The cause of backtrap mottle: Chemical or physical? TAPPI Coating Conference and Trade Fair, Washington, DC, United States, May 1-4, 2000, p. 45

Xiang, Y. and Bousfield, D.W., Effect of coat weight and drying condition on coating structure and ink setting, Tappi Advanced Coating Fundamentals Symposium, San Diego, CA, United States, May 4-5, 2001, p. 35

Yamazaki, K., Nishioka, T., Hattori, Y. and Fujita, K., Print mottle effect of binder migration and latex film formation during coating consolidation, *Tappi Journal*, 76(5), 1993, p.79

Zang, Y.-H. and Aspler, J.S., The effect of surface binder content on print density and ink receptivity of coated paper, *Journal of Pulp and Paper Science*, 24(5), 1998, p. 141

Zimmerman, P.A., Hercules, D.M., Rulle, H., Zehnpfenning, J. and Benninghoven, A., Direct analysis of coated and contaminated paper using time-of-flight secondary ion mass spectrometry, *Tappi Journal*, 78(2), 1995, p. 180

## 6 Appendix

This appendix contains the Raman spectra of several common coating chemicals and polydimethylsiloxane. The detection capability for different chemicals depends on the concentration and the overall coating composition. In general, molecules having weakly polarizable bonds (e.g. starch) are difficult or even impossible to detect in coatings where other compounds give much stronger signals.

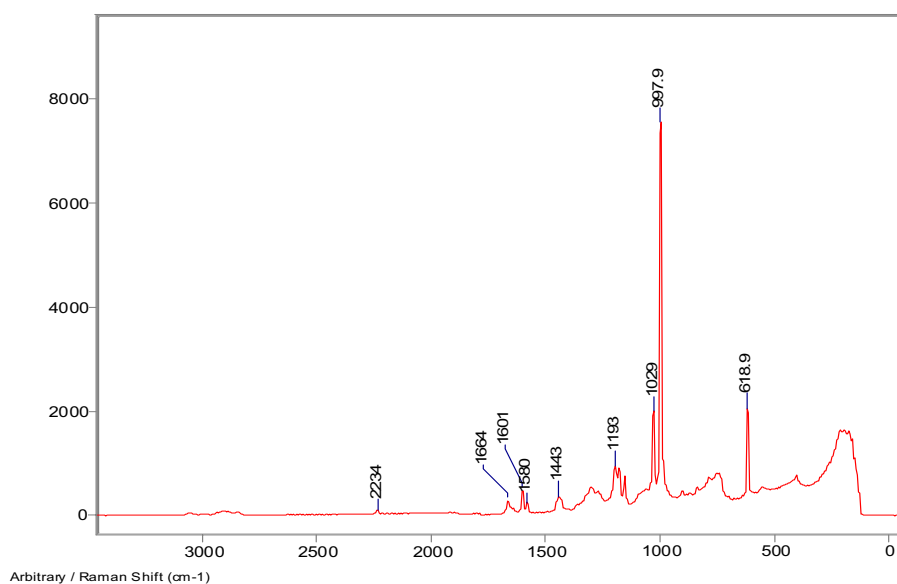


Figure 31. Raman spectrum of SB-latex (Dow, DLL 966). The peak height of the strongest band at  $998\text{ cm}^{-1}$  emerging from the styrene unit was employed in the data analysis. The band at  $1664\text{ cm}^{-1}$  can be assigned to butadiene units.

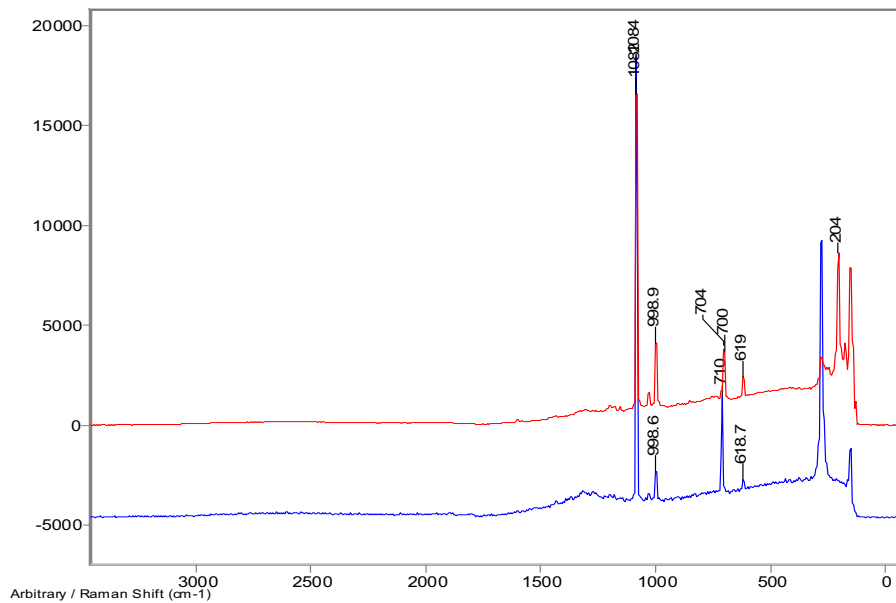


Figure 32. Raman spectrum of typical  $\text{CaCO}_3$  coatings. The lower spectrum is for calcite-type GCC ( $279 \text{ cm}^{-1}$ ) and the upper spectrum for aragonite-type PCC ( $204 \text{ cm}^{-1}$ ). Both Raman spectra show SB-latex bands ( $998 \text{ cm}^{-1}$ ).

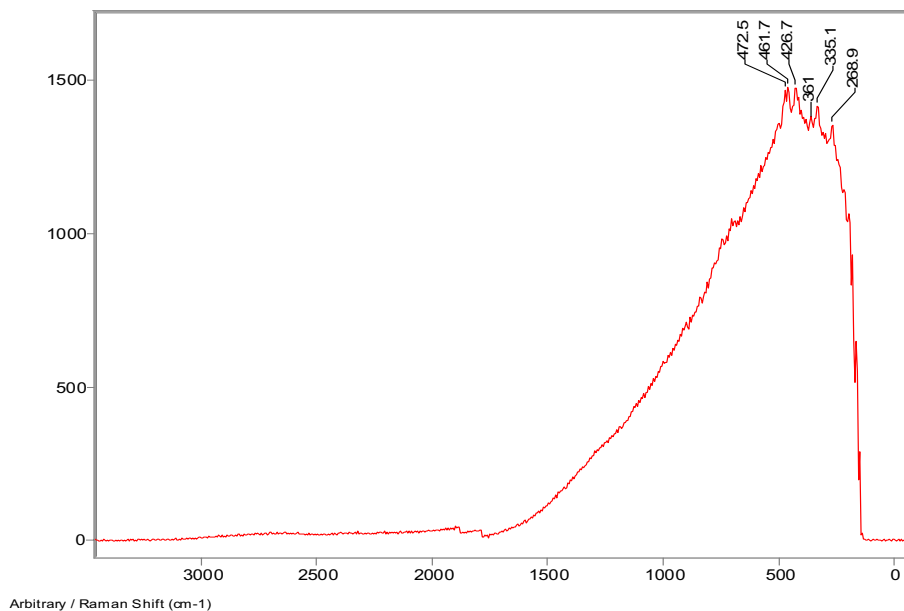


Figure 33. Raman spectrum of kaolin (Imerys, Supramatt).

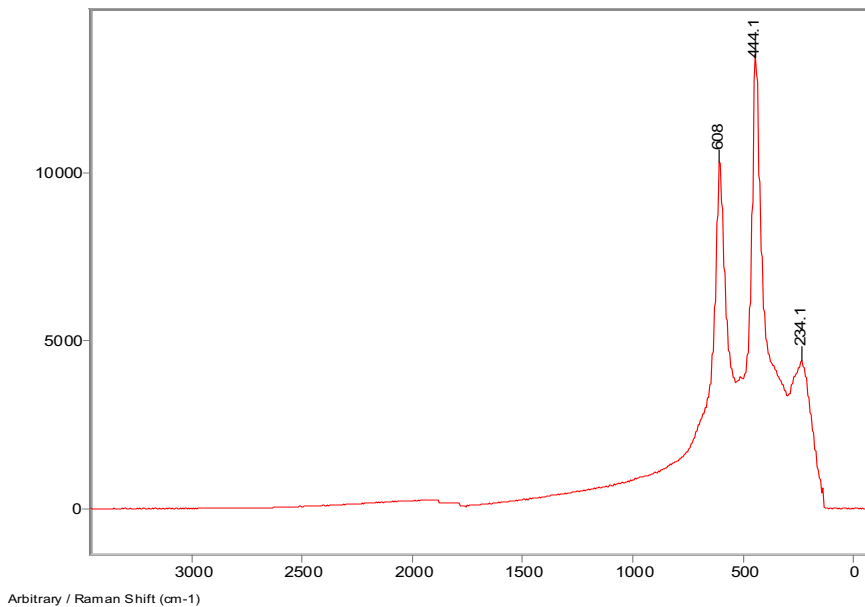


Figure 34. Raman spectrum of  $\text{TiO}_2$  with rutile crystalline form (Kemira, Finntitan RDE 2).

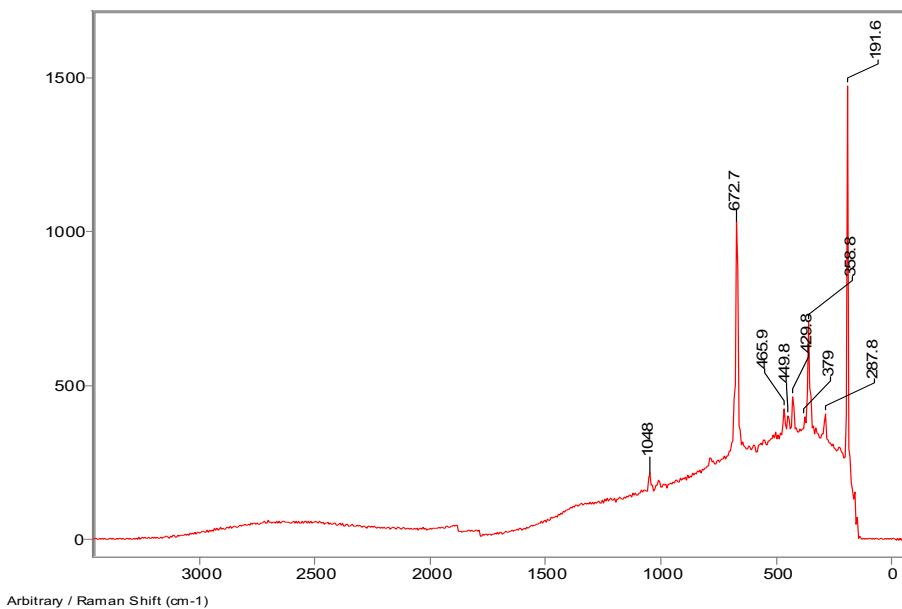


Figure 35. Raman spectrum of talc (Mondo Minerals, Finntalc F10).

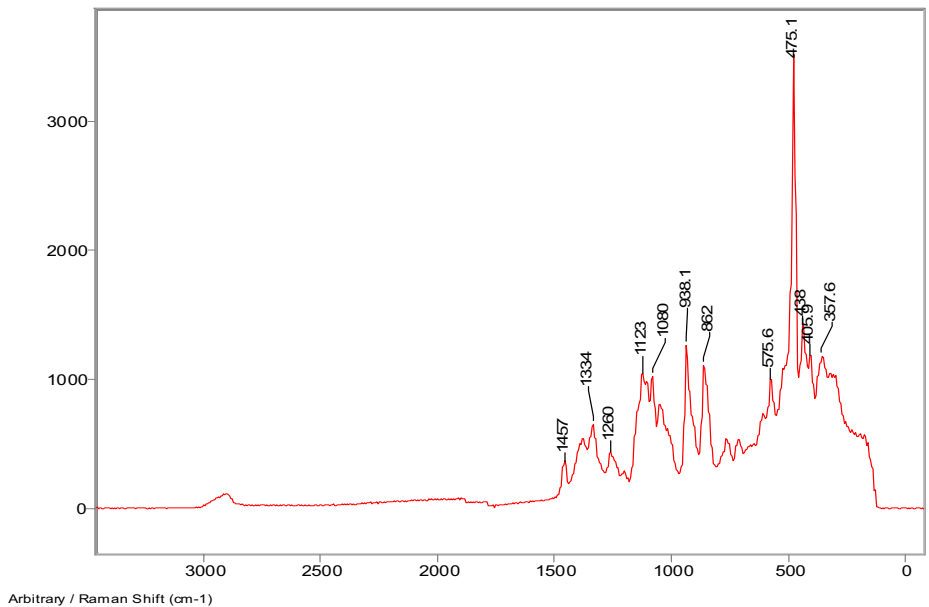


Figure 36. Raman spectrum of starch (Merck, analysis grade).

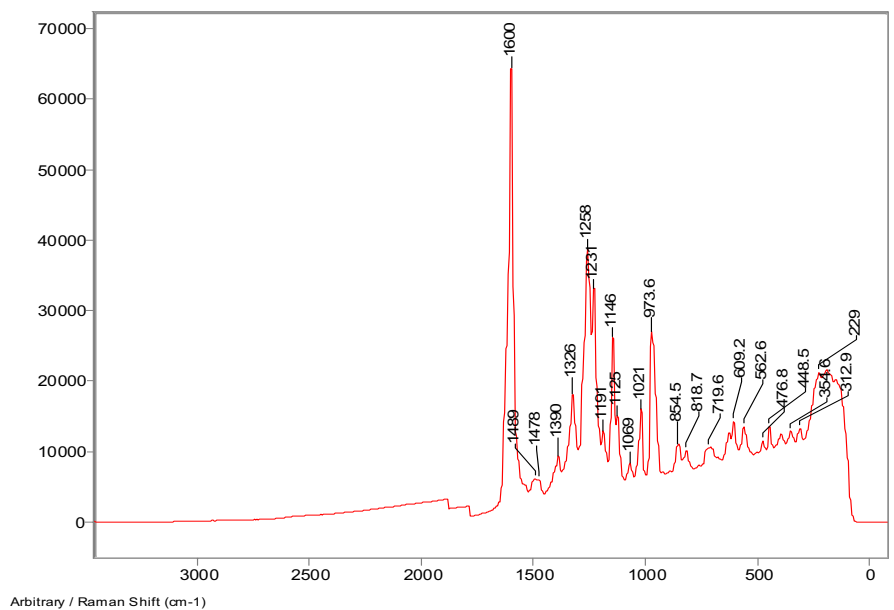


Figure 37. Raman spectrum of optical brightener (Bayer, Blankophor PM).

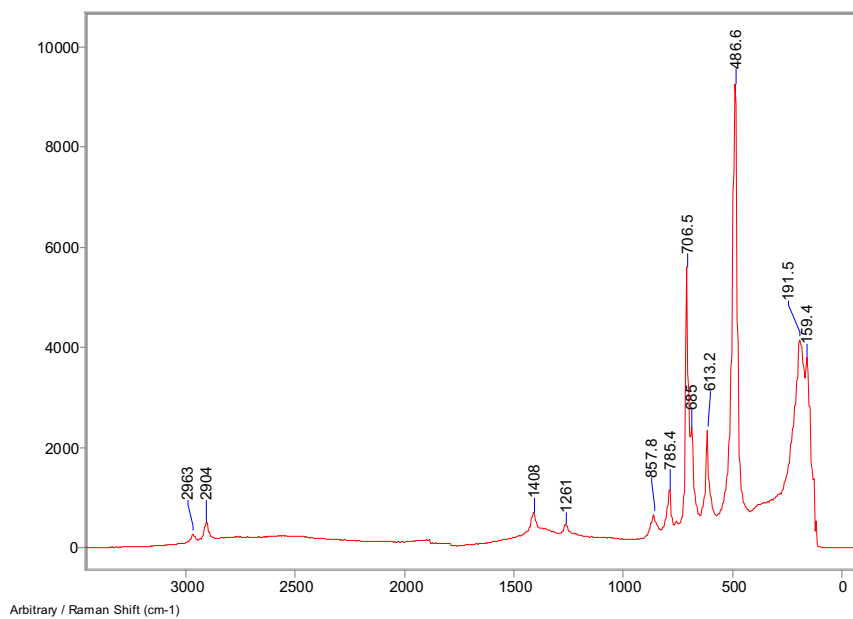


Figure 38. Raman spectrum of polydimethylsiloxane.

HELSINKI UNIVERSITY OF TECHNOLOGY LABORATORY OF FOREST PRODUCTS CHEMISTRY  
REPORTS, SERIES A

1. Laine, J.,  
Surface properties of unbleached kraft pulp fibres, determined by different methods. 142 p. 1994.
2. Merta, J.,  
Interactions between Cationic Starch and Anionic Surfactants. 148 p. 1995.
3. Heimonen, J.,  
The effect of coating components and fillers in the flotation deinking of paper. 148 p. 1995.
4. Mitikka-Eklund, M.,  
Sorption of xylans on cellulose fibres. 84 p. 1996.
5. Laurila, M.,  
The adsorption of nonionic surfactants and polyacrylate on talc. 104 p. 1996.
6. Kekkonen, J.,  
Adhesion properties of polyamide 6 fibers used in press felts. 167 p. 1996.
7. Laine, J.,  
The effect of cooking and bleaching on the surface chemistry and charge properties of kraft pulp fibres. 199 p. 1996.
8. Vikkula, A.,  
Hemicelluloses in kraft cooking liquor. 81 p. 1999.
9. Pirttinen, E., The effect of deinking chemicals in flotation deinking of paper. 50 p. 1999.
10. Vyörykkä, J.,  
Konfokaali-raman-spektrometrin käyttö paperin päällysteen syvyysuuntaiseen analysointiin. 83 p. 1999.
11. Saarinen, T.,  
The surface properties of gels formed by cationic starch and surfactants. 109 p. 2000.

HELSINKI UNIVERSITY OF TECHNOLOGY, LABORATORY OF FOREST PRODUCTS CHEMISTRY  
REPORTS, SERIES A

12. Merta, J.,  
Interactions between cationic starch and anionic surfactants. 107 p. 2001.
13. Haavanlammi, T.,  
Haitta-ainevirrat ja -tasot SC-paperikoneen kierto-vesijärjestelmässä. 121 p. 2001.
14. Kekkonen, J.,  
Adsorption kinetics of wood materials on oxides. 192 p. 2001.
15. Rantanen, M.,  
Solvent retention and fibre chemistry. 225 p. 2002.
16. Räsänen, E.,  
Modelling ion exchange and flow in pulp suspensions. 2003.
17. Kallio, T.,  
Fouling of polymer surfaces in paper machine wet end. 108 p. 2004.